POLITECNICO DI MILANO

School of Industrial and Information Engineering

Department of Energy

CFD-BASED DESIGN AND ANALYSIS OF CENTRIPETAL DISTRIBUTOR SYSTEM FOR AN AXIAL RESEARCH TURBINE

Supervisor: Prof. Giacomo Bruno Persico

Graduation Thesis of:

Gkioun GKIOREN

Matr. n. 780687

Academic year 2012 – 2013

To everyone that helped me during my studies in Politecnico di Milano and during the hard times in my life, but especially to;

Prof. Giacomo Bruno Persico, who was always very helpful and kind,

To my father, who supported me on every stage of my education,

To my mother, who gave me the strength I needed many times,

To my sister, my best friend, the “light” of my life,

To all friends and family members,

And last but not the least, to Kabataş Erkek Lisesi, which played a vital role in my life and made me who I am today

Contents

List of Figures

List of Tables

Abstract

This thesis presents the design work for the inlet guide vanes for centripetal distributor of an axial turbine. The main goal of the work is to maximize the flow uniformity at the outlet of the distributor, also providing an axial flow at the inlet of the test turbine operating the Laboratorio di Fluidodinamica delle Macchine of the Politecnico di Milano. For this purpose, firstly the complete flow region inside the distributor is modeled and simulated to the flow behavior without. Secondly simulations were conducted with a commercial CFD including in the distributor system in presence an Inlet Guide Vane, testing several blade profiles and configurations in order to find an optimum blade profile with regards to both flow behavior (yaw angle) and simplicity for manufacturing. Results from the simulations were analyzed in detail and a certain blade profile and configuration was chosen to be manufactured and to be used in the test rig. Lastly as the spanwise variation of the yaw angle couldn't be prevented in any of the configurations it was decided to introduce a honeycomb structure at the outlet of the distributor to eliminate the residual flow angle and span-wise variation, at the expense of a slight the increase in total pressure loss.

Keywords: CFD, Fluid Dynamics, Inlet Guide Vanes, Turbine, CAD

Chapter 1

Introduction

The design of the fluid machines is one of the most widespread practical engineering applications of the fluid mechanics field. Among these machines the ones that have the most variety are the machines that transfer energy to the fluid, the operating machines. Meanwhile there are also machines that transfer energy from the fluid, called motor machines or turbines. Both of these types are connected to a rotating shaft and named collectively as turbomachinery, derived from the Greek word "τύρβη" (turbulence) and first used as in its modern form by the French mining engineer Claude Burdin in 1822 in his work on hydraulic turbines. Although it was known that pumps and turbines principally existed in ancient times such as Archimedes's screw and windmills the first modern (hydraulic) turbine was built by Benoit Fourneyron, a former student of Burdin in 1827. [1]

In the last decade, the energy industry has been facing major changes mostly because of concerns about sustainability and of course increases in oil and gas prices. Thus, countries worldwide, especially industrialized nations have been forced to look for alternative energy sources in addition to conventional energy resources, in order to decrease the amount of oil dependency and to obtain sustainable industrial development. However, it is a well-known fact that, with current energy technology, it is not possible to reach acceptable energy reliability using Renewable Energy Systems (RES) such as Wind Energy or Solar Energy, due to the difference between the amount of energy needed daily for domestic and industrial use, and output of the RES. Moreover, for the time being, it is not very feasible to increase reliability of such RES, e.g. via energy storage methods, fuel cells and flywheels. Thus, these reasons make it necessary to improve of the efficiency of conventional energy systems such as gas turbines which is a major solution in today's energy market.

The increasing success of gas turbines for industrial applications (both electric and thermal energy production) is mostly due to the technological

progress that are mostly aided by computer based design (specifically by computational fluid dynamics, CFD, and finite element analysis) and by the development of advanced materials that withstand the maximum temperature of the specific cycle that is evermore increasing. This in turn also increases the maximum theoretical thermal efficiency of the cycle. The success of the gas turbines also partly depends on their quick response to load variations; in fact these plants are often used for electric production at partial load between peak and base demand. [2]

Despite the evident and increasing success of turbomachinery and the vital role they play in the fundamental industrial field, there still exist some problems. One of the most common problems is that the operation efficiency is lower than the maximum efficiency. Besides that, generally the need of variable operation at variable conditions arise and the system devices often operate at off-design conditions which needs less pressure ratio. The problem of variable condition demand can be solved, to a certain degree, with frequency control technology and throttle valves. But because the efficiency change in different conditions is not considered in these cases there is still a large gap in pursuit of better efficiency. Thus, the problem of maintaining the high efficiency under different operating conditions with different speeds is yet to be solved in the industrial community. Variable vanes (inlet guide vanes, IGV, and stator blades) are the most common techniques to maintain efficient, stable operation of the turbomachinery. Currently there is a widespread research done on IGV and the papers are mostly focused on the performance effect to the device. Consequently, variable inlet guide vanes (IGV) are now a vital component for the turbomachinery that can optimize performance in a wide range of operating speeds. Additionally, variable inlet guide vanes and adjustable stators are used as an active control method to avoid stall and surge in axial compressors, and they improve the operation effectively in an off-design condition. [3]

As mentioned by Li et. al.; though extensive research about the effect on the turbine performance through simulation and experiment have been done by using IGV, the research on how to adjust IGV to improve efficiency is very rare. [3]

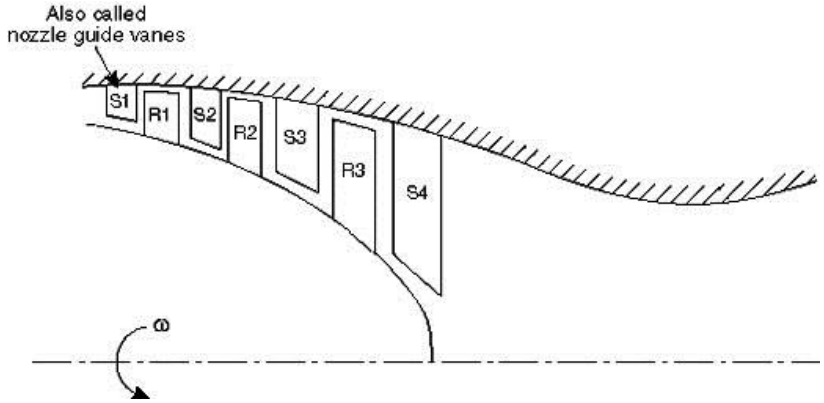

Figure 1.1 Typical inlet guide vane configuration in an axial turbine

In gas turbines the inlet guide vanes adjust the flow coming into the turbine to enhance efficiency and performance in off-design conditions. In an axial turbine IGVs project from the center structure of the inlet, and arranged around the circumference of the turbine inlet, span at least part of the flow path between the inlet inner barrel or center structure and inlet casing and work in concert with the profile of the inlet itself to deliver the flow having desired characteristics (incoming flow direction, speed, direction etc.) to the first rotor of the turbine. In a centripetal distributor, having the same purposes, IGVs can be placed radially in the volute structure.

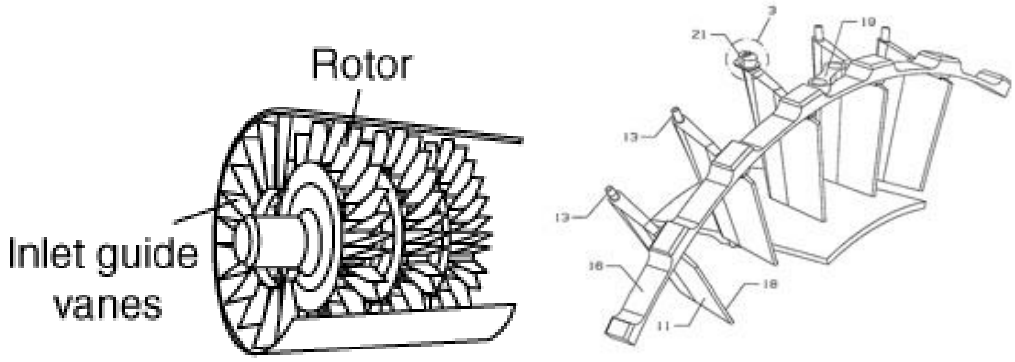

Figure 1.2 Configuration of inlet guide vanes in an axial machine

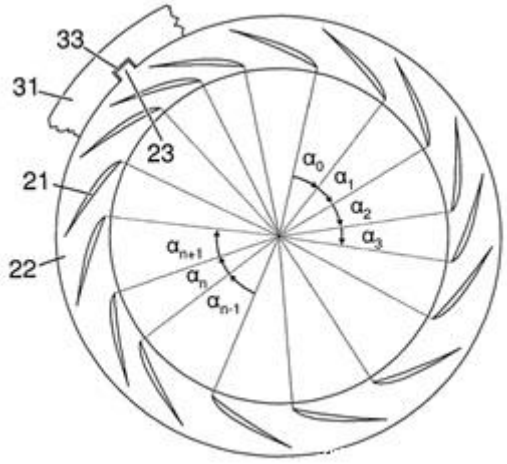

Figure 1.3 Inlet guide vanes in a centripetal machine

In some gas turbines by varying the IGVs' angle of attack the turbine flow rate can be controlled. For example the IGVs in some turbines are mounted on radial shafts that are rotated by actuators in the turbine housing to vary the IGV rotational position and angle of attack. As angle of attack increases incoming flow rate decreases, and as angle of attack decreases incoming flow rate increases. It has been observed that in such variable IGV arrangements, vibration of blades downstream of the IGV can vary significantly with changes in flow setting, which could reduce the turbine and turbine component life. Investigations reveal that a component of the vibration is induced by non-uniform flow separation of the IGVs and that at a reduced flow setting, IGV flow separation becomes very sensitive to inlet flow distortions. As a result, IGVs at some locations experience more flow separation than others and the wakes of IGVs experiencing enhanced flow separation excite certain frequencies of the vibration. [4]

The purpose of this work is to determine a specific profile and angle of attack for the inlet guide vanes positioned inside an existent centripetal volute of an axial turbine that should give a uniform and fully axial flow downstream of the inlet guide vanes and hence at the inlet of the axial turbine stator. The turbine stage will be studied experimentally both from the aerodynamic and aero-acoustic point of views, and hence the uniformity of the flow incoming in the turbine is crucial for a successful experimental campaign.

Chapter 2

Fluid Dynamics Fundamentals and Computational Fluid Dynamics

This chapter covers the fundamental laws of the fluid dynamics which are essential to understand and forms the basis of computational fluid dynamics methods. Following the fundamental laws the important concepts about turbomachinery flow and turbulence modeling are presented. Lastly a brief explanation of the computational fluid dynamics is introduced.

2.1 Fundamental Laws of Fluid Dynamics

The basic governing equations of the fluid dynamics that are needed for the computational methods are the mathematical statements of the conservation laws of physics:

- The mass of a fluid is conserved (the continuity equation).
- The rate of change of momentum equals the sum of the forces on a fluid particle (Newton's second law/the momentum equation)
- The rate of change of energy is equal to the sum of the rate of heat addition to and the rate of work done on a fluid particle (first law of thermodynamics)

2.1.1 The Continuity Equation

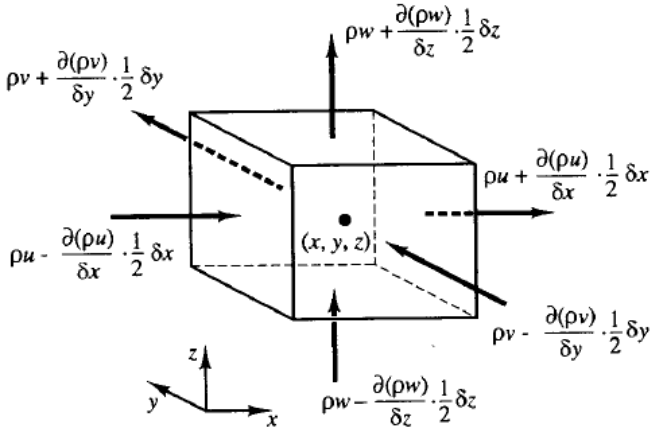

Figure 2.1 Fluid Element [5]

The continuity equation governs the conservation of mass, by requiring that the rate of increase of mass in fluid element is equal to the net rate of flow of mass into fluid element. As all fluid properties are functions of space and time their full notations are ρ(x, y, z, t),

p(x, y, z, t), T(x, y, z, t) and V(x, y, z, t) for the density, pressure, temperature and the velocity vector respectively. Ultimately all terms in the equation are arranged on the left hand side and the equation for unsteady, three-dimensional mass conservation for a compressible fluid is;

$$\frac{\partial \rho}{\partial t} + \frac{\partial(\rho u)}{\partial x} + \frac{\partial(\rho v)}{\partial y} + \frac{\partial(\rho w)}{\partial z} = 0 \qquad (2.1)$$

Or in a more compact form;

$$\frac{\partial \rho}{\partial t} + \nabla \cdot (\rho V) = 0 \qquad (2.2)$$

For incompressible flows as $\nabla\rho = 0$ and $\frac{\partial \rho}{\partial t} = 0$ (constant density in space and time), the equation becomes:

$$\nabla \cdot V = 0 \tag{2.3}$$

In this work the flow will always be considered as incompressible; even though the fluid is air, the maximum Mach number of the streams is always below 0.3, and hence the density variations can be neglected.

2.1.2 The Momentum Equation

Newton's second law or the momentum equation states that the rate of increase or change of momentum of a fluid particle equals the sum of forces acting on the fluid particle. The sum of external forces is equal to the inertia force of the flow. The equation can be written in differential form as below,

$$\rho \frac{DV}{Dt} = f + \nabla p + \nabla \cdot \tau \tag{2.4}$$

In Equation 2.4 f represents the overall effect of body forces which are gravity force, centrifugal force and Coriolis force in case of non-inertial reference frames, and the electromagnetic force. P is the hydrostatic pressure and τ is the viscous stress tensor according to the Navier-Stokes formulation, expressed as:

$$\tau = \mu[\nabla V + (\nabla V)^{\mathrm{T}}] - \frac{2}{3}\mu \nabla \cdot VI \tag{2.5}$$

Viscosity, μ has to be properly corrected for a turbulent flow field, so an extra focus is needed for its definition. A new term called eddy viscosity, μ_e is defined with the addition of turbulent viscosity, μ_t and can be formulated as:

$$\mu_e = \mu + \mu_t \tag{2.6}$$

2.1.3 The Energy Equation

The energy equation, derived from the first law of thermodynamics states that the rate of change of energy of a fluid particle is equal to the rate of heat added to the particle plus the rate of work done on the particle.

By multiplying Equation 2.4 by *V* it is possible to formulate:

$$\rho \frac{D}{Dt}\left(\frac{V^2}{2}\right) = f \cdot V + \frac{Dp}{Dt} + \frac{\partial p}{\partial t} + V \cdot (\nabla \cdot \tau) \qquad (2.7)$$

which expresses the conservation of the mechanical energy. By introducing the fundamental relation of thermodynamics:

$$\rho \frac{dh}{dt} = \frac{dp}{dt} + \rho T \frac{ds}{dt} \qquad (2.8)$$

An ultimate equation is formulated as ;

$$\rho \frac{Dh_T}{Dt} = \rho f \cdot V + \rho T \frac{Ds}{Dt} + \frac{\partial p}{\partial t} + V \cdot (\nabla \cdot \tau) \qquad (2.9)$$

that expresses the energy conservation.

2.1.4 Radial Equilibrium

The streamlines in an annular duct cannot be counted as parallel to axis, due to the geometry of the meridional flow path and the strong bending caused by it. Thus it is important to introduce the definition of Radial Equilibrium that is the governing law for the flow behavior in annular turbomachinery channels. According to radial equilibrium in for a fluid element in an annular channel section which can be seen in Figure 2.2, there must be a pressure gradient that balances the centrifugal forces.

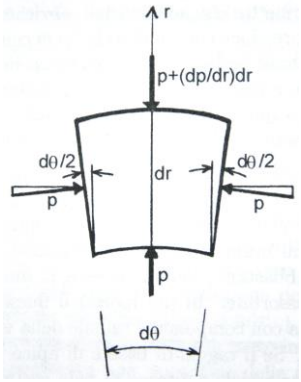

Figure 2.2 Radial equilibrium [6]

It is assumed that the flow is steady, purely cylindrical and axisymmetric in the analysis. This hypothesis is possible when the wakes or vortices produced

by the airfoils are not taken into account thus when an axial machine in a normal-to-axis plane, far enough from stator vanes and rotor blades is considered. This assumption makes the radial velocity V_r and W_r components negligible. Then the radial equilibrium can be formulated as below:

$$V_a \frac{dV_a}{dr} + \frac{V_t}{r} \frac{d(rV_t)}{dr} = 0 \qquad (2.10)$$

Considering a small fluid element with mass dm, unit depth dz and subtending an angle $d\theta$ at the axis, rotating about the axis with tangential velocity Vt at radius r, it can be said that the element is in radial equilibrium and the pressure forces are equal to the centrifugal forces such as:

$$\left(p + \frac{dp}{dr} dr\right)(r + dr)dzd\theta - prdzd\theta - 2pdrdzsin\frac{d\theta}{2} = r\frac{dp}{dr} drdzd\theta \qquad (2.11)$$

where dm is defined as dm = ρdθdr.

This force, generated by the pressure gradient, has to balance the centrifugal force of the fluid element: $rdrdzd\theta\rho\frac{V_t^2}{r}$ and ignoring terms of the second order of smallness, the above equation becomes:

$$\frac{1}{\rho}\frac{dp}{dr} = \frac{V_t^2}{r} \qquad (2.12)$$

To solve Equation (2.10 or 2.12), either one of the two unknown velocity components (V_a and V_r) or a relation between is needed to be known, which leads to two different approaches that can be applied:

Direct problem, where the whole geometry is known, and with it the flow angle variation, determined by the angle α is also known. V_t, V_a and the pressure distribution can be determined by solving the radial equilibrium.

Indirect problem, where one of the fluid dynamics variable is assigned (i.e $V_t(r)$). The radial equilibrium equation allows the solution of the other variables and the geometry.

2.2 Turbomachinery Flow Features

Flow in turbomachinery is fully three-dimensional as the aspects of internal and external flows merge together. Aerodynamic, viscous and turbulent effects play a major role in flow characteristics such as; pressure distribution along the blade sides, boundary layer development along the blade sides, wake shed by the trailing edge (which are the aspects of external flow), mean flow deflection, boundary layer development on the endwalls, secondary flow development at the endwalls (which are aspects of internal flow in the turbomachinery flow). In addition to these phenomena transonic and supersonic flows are also commonly found in turbomachinery. In the Figure 2.3 typical phenomena that can be seen in turbomachinery flow are presented.

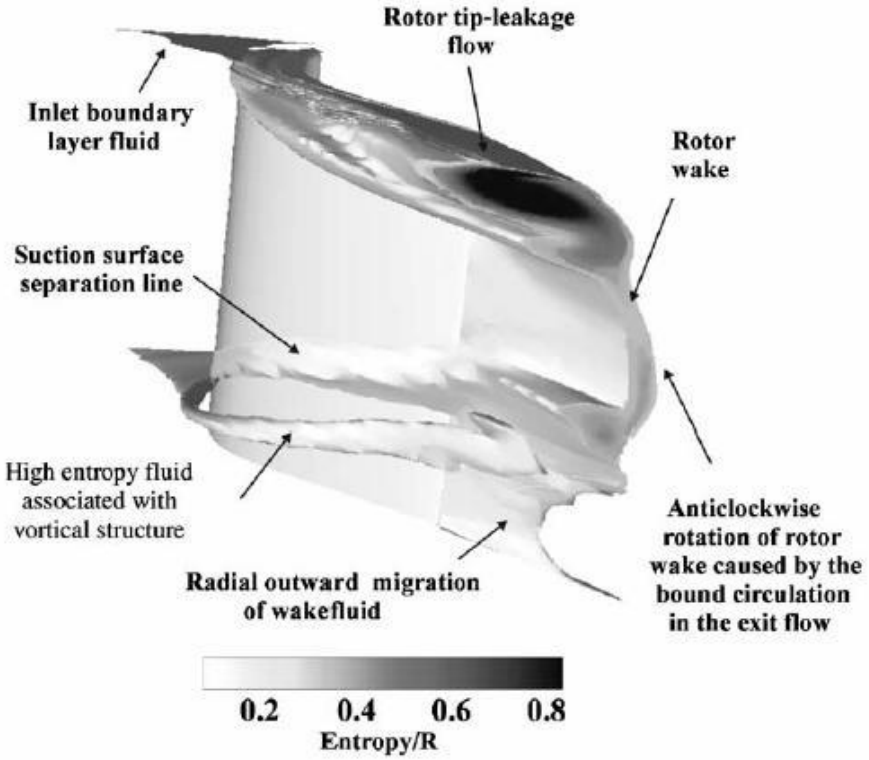

Figure 2.3 Phenomena in Turbomachinery Flow [9]

Generally during the study of flow in turbomachinery two different types of planes are used. These planes are called meridional surface which represents the channel between the endwalls and blade-to-blade surface which contains the blade profiles in a row that are represented below in the Figure 2.4.

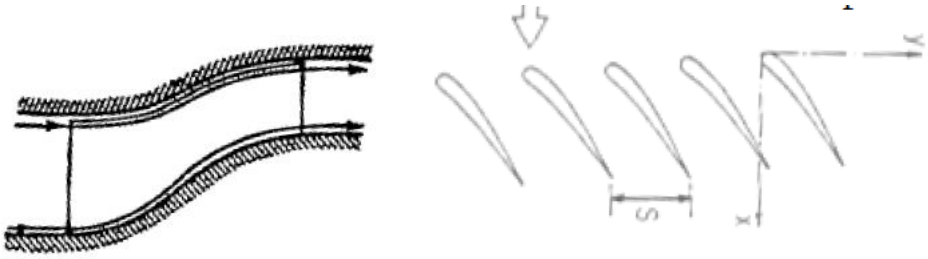

Figure 2.4 Meridional and Blade-to-Blade Surfaces

2.3 Throughflow Methods for Flows in Turbomachinery

Channel Method: This method evolved from the early radial equilibrium approaches and is a quasi-3D solution based on generalized radial equilibrium including, spanwise total enthalpy and entropy gradients which lead to Euler work and correlations, and spanwise streamline curvature which is the source term that forms the continuity equation. The formulation of the channel method gives;

$$V_a \frac{\partial V_a}{\partial r} - V_a \frac{\partial V_r}{\partial z} + \frac{V_t}{r} \frac{\partial (r V_t)}{\partial r} = \frac{\partial h_T}{\partial r} - T \frac{\partial s}{\partial r} \qquad (2.13)$$

Streamline Curvature Method: Is a method where radial equilibrium equation account for much more features. The equation for this method () is written in inherent streamwise (m) and normal (q) coordinates. Stream surface orientation is in circumferential (γ) and radial (ψ) directions and viscous losses are addressed with a “drag” volume force.

$$c_m \frac{dc_m}{dq} = \frac{dh_T}{dq} - T\frac{ds}{dq} - \frac{1}{2r^2}\frac{d(r^2 c_u^2)}{dq} + sin\psi \frac{c_m^2}{r_c} + cos\psi c_m \frac{\partial c_m}{\partial m} + tan\gamma \frac{c_m}{r}\frac{\partial (r c_u)}{\partial m} + F_d \quad (2.14)$$

Where mass conservation is also defined as,

$$\dot{m} = \int k\rho c_m sin\psi dq \quad (2.15)$$

k, is the empirical blockage factor.

This method has its limitations in the strong effect of the orientation of the streamsurface and its inability to treat choked flows.

Computational Fluid Dynamics-based conservative Method: This approach has two types as 2D and 3D. 2D approach which is bridging the 1D and 3D methods projects the mean surfaces of the blades to meridional plane, while in 3D approach blades are replaced by mean surfaces and axisymmetric flow is assumed.

In the CFD-based throughflow methods any flow quantity is averaged in circumferential direction,

$$\bar{\alpha}(x,r) = \frac{1}{\theta_p - \theta_s}\int_{\theta_s}^{\theta_p} \alpha(x,r,\theta) d\theta \quad (2.16)$$

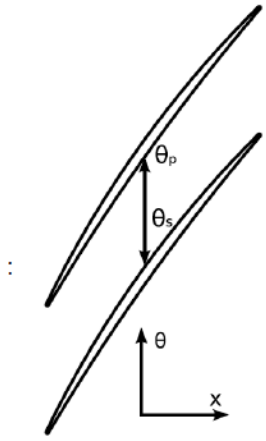

Figure 2.5 Circumferential View

The strength of this method is the fact that it has a very simplified approach. On the other hand key information on the blade-to-blade plane is lost related to the imposition of flow deflection in the blade-to-blade plane and the effect of profile loss.

Blade-to-Blade Model: Blade-to-blade model is strictly based on external flow problem. The equations are averaged in spanwise direction,

$$h\frac{\partial U}{\partial t}+\frac{\partial (hF)}{\partial x}+\frac{\partial (hG)}{\partial y}=S \qquad (2.17)$$

Its most typical difference with respect to an isolated airfoil problem is that the profiles are assembled in cascades. That means if the identical blades are assembled with a constant pitch then the periodic conditions can be assigned to lateral surfaces resulting in the requirement of solving just one blade channel which in turn means huge savings in computational cost.

Typical set of boundary conditions in a blade-to-blade model are

- The flow in the turbomachinery is rarely entirely supersonic
- Total pressure, total temperature and flow angles are assigned at domain inlet; and static pressure at domain outlet
- Periodic boundary condition at lateral surfaces, with no-slip and no-heat transfer at blade wall

2.3.1 Periodicity conditions

If the identical blades are assembled with a constant pitch P, which means that they are in a cascade then the solution repeats itself for each pitch distance, or it is periodic in space of period P:

$$U(x, y, t) = U(x, y + P, t) \qquad (2.18)$$

It is sufficient to achieve the solution for a single spatial period to achieve global solution by application of periodic boundary conditions on lateral surfaces. It is also not important how the periodic line is defined, but it is necessary that the grid is identical on periodic surfaces.

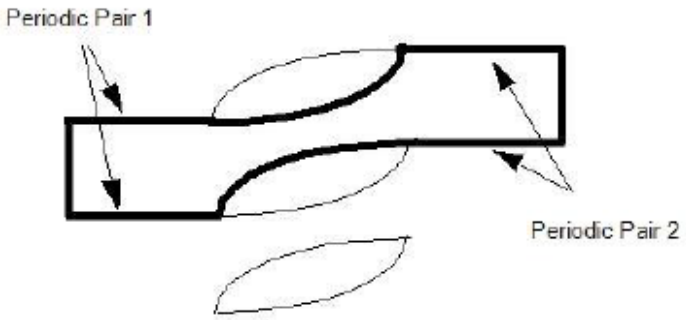

Figure 2.6 A Periodic Blade Channel

2.3.2 Transonic Flows

A cascade is defined as transonic if only either inlet or outlet is supersonic. In transonic turbines the inlet is subsonic and the outlet is supersonic. Meanwhile in transonic compressors the inlet is supersonic and the outlet is subsonic.

2.4 A Brief Analysis of an Aerodynamic Problem

The main goals behind an aerodynamic analysis are;

Either wall quantities:

- Pressure distribution on the profile/blade walls (existence of shocks)
- Wall shear stress on the profile/blade walls (existence of transition and flow separation)
- Temperature distribution or wall heat transfer on the profile/blade walls

Or flow features such as:

- Boundary layer state and development along the profile/blade, including evaluation of displacement thickness, momentum thickness and shape factor
- Wake development and mixing process downstream of the blade trailing edge
- Identification of transonic/supersonic regions
- Presence of severe pressure gradients and/or shock waves (shock strength)
- Analysis of total pressure field downstream of the object, to quantify the losses

The boundary conditions of the material boundary which is the wall contouring the profile, in an aerodynamic problem are:

- No-slip velocity conditions (V_w=0) in case of viscous/turbulent flows
- Either wall heat transfer rate (Neumann BC, $\partial T/\partial y|_W$) which is in most cases zero ($\partial T/\partial y|_W$ =0) as wall is assumed to be adiabatic
- Or wall temperature (Dirichlet BC, T_w) for high pressure blade heat transfer studies

Concept of well posedness: A problem is well posed if the solution exists and is unique. In aerodynamics, it is necessary to consider the properties of the flow regime to reach well posedness. Subsonic flows need either 3 (for 2D problems) or 4 (for 3D problems) boundary condition at inlet and 1 at outlet, which are typically inlet total pressure/temperature, flow angle and outlet pressure. Supersonic flows either need 4 (for 2D) or 5 (for 3D) boundary conditions for

the inlet and they are typically inlet total pressure/temperature, static pressure and flow angle.

In turbomachinery blade rows, sometimes (e.g., for compressor cases) the mass flow rate is preferred to be assigned instead of the outlet pressure, but this can result in failed convergence for transonic problems, in which a maximum (chocking) flow rate exists.

For lateral boundaries either (or at the same time) no-slip, symmetry or periodic condition can be assigned. As mentioned before for the periodic surfaces of the turbomachinery that periodicity is assigned full grid correspondence at boundary is required in order to avoid interpolation errors.

2.5 Turbulence Modelling

Turbulence is a three-dimensional, unsteady, rotational, fluid motion with broad-banded fluctuations of flow quantities (such as velocity, pressure, temperature) occurring in both time and space. The non-linearity in the governing equations of the flow is the physical origin of the turbulence concept (Navier-Stokes equations).

Turbulence greatly increases the rates of momentum, heat, and mass transfer and is triggered by the fluid-dynamic instabilities that for a Reynolds number beyond a certain limit (specific for the problem) break the regular laminar profiles leading to the formation of unsteady vortices. Friction and drag forces, wall heat flux, mixing also are largely dependent on turbulence level.

Instability in flow affect the newly formed structures, rapidly leading to a chaotic flow motion which is theoretically impossible to predict and combined with the fact that most flows in the nature and nearly all flows of practical engineering interest are highly turbulent (such as the turbomachinery and internal combustion engine flows) a great deal of effort for turbulence modeling is required.

There are five main properties that characterize a turbulent flow:

1. Fluctuations: flow quantities exhibit chaotic fluctuations even in presence of time-invariant boundary conditions
2. Non-linearity: turbulence is caused by the non-linear nature of the Navier-Stokes equations, and is triggered by sufficiently higher values of non-linearity parameters (such as Re). Turbulence is, in fact, the final state of a process composed by a succession of non-linear instabilities, called *transition*.
3. Vorticity: turbulent flows are characterized by a fluctuating vorticity; highly unstable streaks and swirls, called *eddies*, undergo distortion and spin; the eddy size ranges from the problem length scale to very small scale (the larger the Re, the smaller the scale)
4. Dissipation: momentum is transferred from larger to smaller eddies, until viscous dissipation occurs at the level of the smallest eddies
5. Diffusivity: the chaotic motion enhances mixing via transport, resulting in mass, momentum and energy diffusion rates much larger than molecular ones [10]

2.5.1 Turbulence Models in Use

1. Reynolds averaged Navier Stokes equation model:

$$\frac{\partial(\rho e_t)}{\partial t} + \nabla \cdot \left(\rho h_t \vec{V}\right) = \rho \vec{g} \cdot \vec{V} + \vec{V}\nabla \cdot \bar{\bar{\tau}} + \varepsilon + k\nabla^2 T \qquad (2.19)$$

Where $e_t = e + V^2/2$,is total internal energy

ε is called dissipation function which accounts for the destruction of kinetic energy due to molecular diffusion (conversion into internal energy)

k is the thermal conductivity

For turbulent boundary layers the law of the wall governs the flow behavior which states that the average velocity of a turbulent flow at a certain point is proportional to the logarithm of the distance from that point to the "wall", or the boundary of the fluid region It is only technically applicable to parts of the flow that are close to the wall (<20% of the height of the flow), and a dimensionless parameter called y^+ governs the velocity profile in the wall region of the boundary layer which is defined as; [11]

$$y^+ = \frac{u_* y}{\nu} \tag{2.20}$$

Where, u_* is the friction velocity at the nearest wall, depending on the wall shear stress and the fluid density, y is the distance to the nearest wall and ν is the local kinematic viscosity of the fluid.

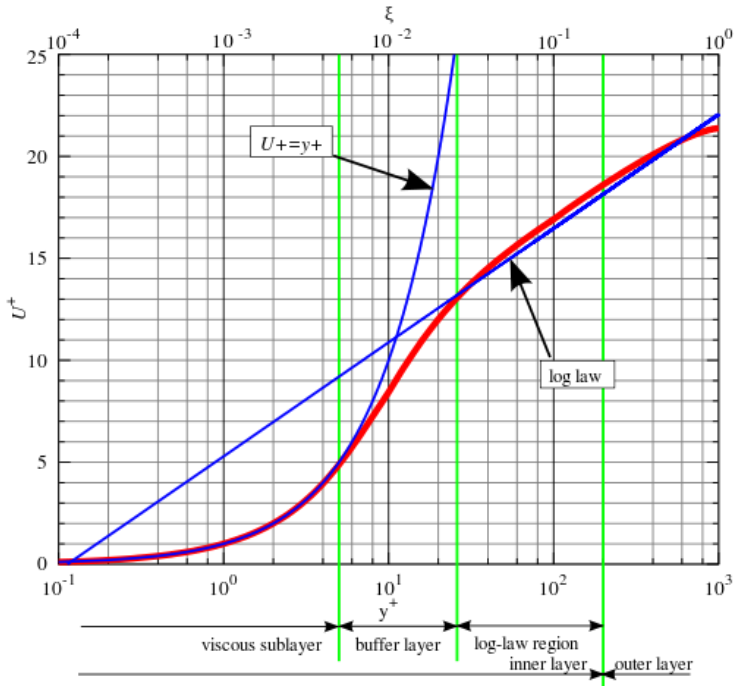

Figure 2.7 Law of the wall and boundary layer subregions

- y+ < 5 ÷ 10 : linear viscous sublayer
- 30 < y+ < 3000 : logarithmic layer
- 10 < y+ < 30 : buffer layer

Some turbulence models exhibit problems for turbulence solutions at the wall. They make use of so-called wall functions, (the law of the wall) and solve for the turbulence quantities starting from a certain wall distance. The CFD simulation of a turbulent flow strongly relies on the wall functions, if they are used, and full coherence between the grid and the model is required to achieve reliable results.

2.One Equation Models:

- Prandtl mixing length concept
- Spalart-Allmaras (S-A)/Baldwin-Barth Models

1. Two Equation Models

k-ε Model: The most famous and applied model, present in any commercial CFD code, equation dependent on k, turbulent kinetic energy and ε its dissipation rate.

This model guarantees acceptable accuracy for simple flows while it is problematic in the near wall region, so wall functions must be used.

k-ω Model: This model requires less tuning compared to k-ε Model. It is much better for the near wall region and wall functions can be used just when it is needed to reduce computational time. It is also much better in boundary layer with pressure gradients and in presence of separation whiles less accurate and more problematic in the treatment of free-stream turbulence

The performance of present-day turbulence models, namely, S-A , k-ε and k-ω are heavily dependent on the grid refinement at the wall and proper mesh clustering is necessary close to the walls. When building a proper mesh one must take into account that S-A model depends explicitly on the distance from the wall, k-ε is problematic at the wall and k-ω doesn't suffer from near wall singularity and offers to solve directly the boundary layer. Sufficient mesh clustering near the wall for different models are defined below as,

i) or S-A and k-ω, which have the chance to solve the boundary layer up to wall:
   - $y^+ = 1$ at the wall
   - At least 10 cells in viscous sublayer

ii) for k-ε, which is problematic at the wall, solving it up to a certain distance and requires wall functions
   - $y^+ = 50 - 500$ at the wall
   - About 10 cells in boundary layer

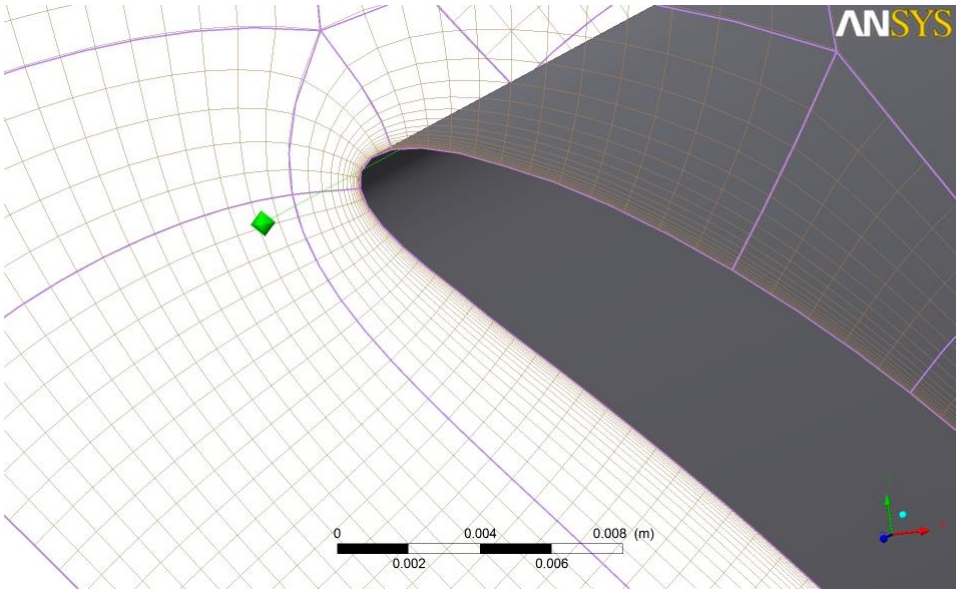

Figure 2.8 Mesh refinement near the wall

2.5.2 Selection and setting of turbulence model

The selection of turbulence model depends on:

- Objective of the calculation: initial design, refined design, problem analysis
- Expected reliability / fidelity level
- Experience available on similar problems
- Correspondence between the model and problem

The selection of turbulence model affects the whole calculation as the grid must be coherent with the model in regions of severe gradients (wall y+) and proper boundary conditions must be set to the turbulence model equations

Turbulence model has a very strong effect on the calculation process, slowing down the convergence process and often inducing stability problems; higher grid resolution can lead to better result but also at the same time often complicates the solution procedure

Turbulence model directly governs some flow features such as boundary layers, viscous drag, wall friction, wakes and secondary flows; but has a much weaker effect on other ones such as lift, pressure distribution and pressure drag. This is an issue that has to be carefully considered as in cases where only the pressure distribution is required, there is no need for complex turbulent calculation.

Also wall treatment is crucial as the use of wall functions results in significant savings in calculation time and complexity, but also in reduces the accuracy of the calculation.

Turbulence models also affect well posedness as it is achieved by assigning k and ε or k and ω at the domain inlet.

2.6 Computational Fluid Dynamics

During the last decade with the help of advancing computational technology a new method for design appeared in the field of fluid dynamics of turbomachinery which can be commonly named as numerical approach or more specifically Computational Fluid Dynamics (CFD). As this work is mostly based on this approach a brief introduction to CFD is presented to give an insight to the working principles of this method.

The computational fluid dynamics is the present day state-of-art technique in fluid flow analysis. It has wide range of applications like aerodynamics of aircraft and vehicles, flow analysis of turbo-machinery, hydrodynamics of ships, power plants, automobiles, process industries, marine engineering, biomedical engineering etc. [12]

CFD has many advantages compared to experimental research, like the ability to simulate the behavior of flow in a system with different operating conditions or creating and setting up new configurations for a specific purpose with much lower research cost and time. Besides unlike in experimental works, where measuring devices may disturb the flow path and restrict the extraction of reliable data, CFD gives detailed information along the whole flow path without any external effects. All those reasons make CFD a very feasible research method both for academic field and engineering companies who cannot always afford experimental set-ups. Indeed, the development costs for a gas turbine

engine can easily exceed £0.5 billion. Typical compressor rig tests can cost around £0.75 million. These extreme costs mean that there is an ever-increasing reliance on CFD and strong economic drivers for this. [13]

Nevertheless, CFD is a method that actually creates a simulation of the reality unlike experiments which are directly real situations. So data reduction is very critical when resorting to a CFD application and a good knowledge in fluid mechanics is required.

2.6.1 Computational time

Computational time is one of the most important aspects in a CFD calculation. The time required to get a solution is highly dependent on the situation that was modeled. In the Direct Numerical Simulations (DNS) the Navier-Stokes equations are solved directly without the application of turbulence models, which doesn't permit the method to be used in industrial work as very large memory storage is required.

Instead, Large Eddy Simulations (LES) can also be used for turbulent flows, in which larger scales of turbulence are solved and smaller scales of turbulence are modeled by the addition of a subgrid viscosity. Nonetheless, LES method also requires large memory storage due to the high computational time, which isn't feasible for the industrial applications. By using the Reynolds Averaged Navier Stokes (RANS) and Favre Averaged Navier Stokes (FANS) ,two frequently used methods in CFD, it is possible to reduce the required memory storage space and thus make CFD feasible for industrial applications.

The logic of CFD is established on the solution of the fundamental laws of the fluid dynamics: the continuity equation, the momentum equation (three separate scalar equations for three dimensional Cartesian coordinates) the energy equation and the state equations below;

$$\rho = f(p,T)\ ; \qquad u = u(p,T) \tag{2.21}$$

which can be written for the perfect gases as;

$$p = \rho RT\ ; \qquad u = c_v T + K \tag{2.22}$$

After defining the main characteristics of the flow, the model geometry and the boundary conditions that are needed, the fluid dynamics equation

system that defines the problem can be written. But the system of equations can be solved analytically only in a small number of simplified applications. In more general fluid dynamics problems it is not possible to achieve an analytical solution due to the non-linear nature of Navier-Stokes equations.

These limitations create the need to find a different method to search for the solution, which is based on finding an iterative numerical solution with the help of approximation of differential equations. The system of fluid dynamics equations is simplified and solved by iterations within a discretized domain, and final solution is found.

The analytical approach allows the governing equations to be applied to an infinitesimal domain before being integrated for the whole domain. On the other hand with a numerical approach this is no longer possible as defining an infinitesimal domain is impossible in a computational method. In turn the entire domain is discretized and small subdomains called cells are formed and altogether these cells form the mesh.

Also due to the time-marching nature of the calculation, care must be placed on the time-step setting. The non-linearity of the equations can lead to numerical instability either at the beginning of the calculation or if there are very small cells present in the grid, even though being implicit.

During the calculation the first quantities that should be taken into account are equation residuals. Convergence process is normally measured by the reduction in orders of magnitude of residuals. However low residuals don't mean that the result converge always and so it is possible that even for low residuals the steady state may not be reached.

Once the convergence is achieved, the computed solution must be processed to evaluate the quality and reliability of the result. The quality of the results is first determined by the near wall behavior, y^+ must be similar to its estimated value. The absence of reflections, appearing as pressure waves is also an indication of the quality of the result. Quantities must be checked to evaluate the outcome, e.g on a turbomachinery blade channel the assigned value was outlet static pressure the mass flow rate must be verified.

2.6.2 The working principles of a CFD code

CFD codes are composed of numerical algorithms that are used to solve fluid dynamic problems. All commercial CFD softwares include detailed interfaces for the user to create the input files and analyze the results with the aim of easy access and increasing the solving power. Usually a CFD code contains three main parts: a pre-processor, a solver and a post-processor. The function of each part is briefly explained below;

2.6.3 Pre-Processor

The pre-processing contains the input of the problem to a CFD program with the help of an easy-to-use interface and the subsequent transformation of this input into a form suitable for the solver. Pre-processing stage contains following activities:

- Definition of the geometry of the problem or the computational domain
- Grid generation: sub-division of the domain into a number of smaller, non-overlapping sub-domains
- Selection of the physical phenomena to be modeled
- Definition of the fluid properties
- Specification of appropriate boundary conditions at the domain boundary

The solution of a fluid dynamics problem is established at the nodes inside each cell and the overall accuracy of the solution is dependent on the number of cells in the grid. Generally accuracy of the solution increases with the number of cells, but the fineness of the grid also increases either computational time or the cost of the necessary computer hardware. It should be noted that optimal meshes are frequently non-uniform: finer in areas where large variations in fluid behavior occur in small distances and coarser in areas where relatively little variation exists. Generally the trade-off in the design of a grid between accuracy and solution time is up to the skills of the CFD user and the available computer hardware.

2.6.4 Solver

There are four different types of numerical solution methods: finite difference, finite element, spectral methods and finite volume methods. Following actions are done by the numerical methods that form the base of the solver:

- Approximation of the unknown problem variables by means of simple functions
- Discretisation by substitution of the approximations into the governing fluid dynamics equations and mathematical subsequent mathematical manipulations
- Solution of the algebraic equations

The main differences of the three numerical solution methods mentioned are related with the way in which the variables are approximated and also with the discretization process.

Finite difference methods: In finite difference methods the unknowns of the problem are defined with point samples at the nodes of a grid of co-ordinate lines. To generate finite difference approximations of the derivatives of the unknowns at each point generally truncated Taylor series expansions are used. Then these finite differences replace the derivatives in the governing equations resulting in an algebraic equation for the values of the unknowns at each point.

Finite Element Method: Simple piecewise functions (e.g. linear or quadratic) that are valid on elements are used in finite element methods to define the local variations of problem unknowns. As the governing equation is satisfied only by the exact solution, the piecewise approximating functions, when substituted into the equation, will not hold exactly and a residual will appear which will indicate the error. Thus a set of algebraic equations is obtained for the unknown coefficients of the approximating functions after the minimization of the errors or the residuals. The theory of finite elements has been developed initially for structural stress analysis.

Spectral Methods: Unknowns are approximated by truncated Fourier series or series of Chebyshev polynomials. Unlike the two other methods, approximations are valid for entire computational domain, not just locally. Unknowns are again replaced by truncated series in the governing equation and

the algebraic equations are formed by similar way as in the finite element method.

The finite volume method: This method was originally developed as a special finite difference formulation and now it's the most well-established and thoroughly validated CFD technique that is the base for most of the commercial CFD codes. Its numerical algorithm consists of:

- Integration of the fluid dynamics governing equations over the computational domain
- Discretization, where substitution of approximations for the terms in the equations representing flow behavior takes place and this transforms the integral equations into a system of algebraic equations
- Solution of the algebraic equations by iteration

Finite volume method is distinguished from other methods by its first step of integration. For each cell in the computational domain the exact conservation of the relevant properties are defined by the resulting statements. Because of the clear relationship between the numerical algorithm and the physical conservation principles this method is much easier to understand by engineers compared to other methods and can be naturally formulated in conservative form.

2.6.5 Post-Processor

Most of the commercial CFD software include following versatile data visualization tools with high graphics capabilities due to a large amount of development that took place in post-processors:

- Domain geometry and grid display
- Vector plots
- Line and shaded contour plots
- 2D and 3D surface plots
- Particle tracking
- View manipulation
- Recently, animation for dynamic result display etc.

2.7 ANSYS CFX

Simulations of this work were performed by ANSYS CFX which is a general purpose CFD software suite that contains an advanced solver with powerful pre- and post-processors. The suite contains four main modules besides several toolboxes that take the geometry and mesh and pass the information required to perform a CFD analysis:

- TurboGrid, the mesh generator
- CFX-Pre, the pre-processor where multiple meshes may be imported, allowing analyses of complex geometries that consist of flow physics, boundary conditions, initial values and solver parameters
- CFX-Solver, the solver which is a coupled solver that allows the hydrodynamic equations to be solved as a single system with fewer iterations and a shorter computational time
- CFX-Post, the post-processor which allows the generation of several reports and visual data output

Also during the work Flowizard as a separate mesh generator software was used for the first part of the work; and the geometry of the computational domain required by the CFD analyses was created by using SolidWorks, a widespread solid modeling software.[14]

Chapter 3

High Speed Closed Loop Test Rig for Axial and Radial Stages

This section will explain briefly the test rig that contains the centripetal volute on which this work is focused. For the aim of research programs on axial turbines and centrifugal compressors a closed loop test rig for axial and centrifugal turbomachines has been launched in 2001 at Laboratorio di Fluidodinamica delle Macchine (LFM).

With reference to Figure 3.1, the test rig is equipped with a section for centrifugal turbomachines (ref. 1) followed by a cooling section (heat exchangers) (ref. 3, 4), a Venturi nozzle for the flow rate measurement (ref. 5) and a filtering section (ref. 10); the pressurized flow rate can be exhausted either in the by-pass line or in the axial section (ref.2).

Flow rate regulation can be performed by two throttling valve sections (ref. 9, 10). The test rig can be operated under closed conditions or forcing the outlet or the inlet of the axial section to the atmospheric pressure; as an alternative the compressor can be connected to other LFM facilities through connection 6 and 7.

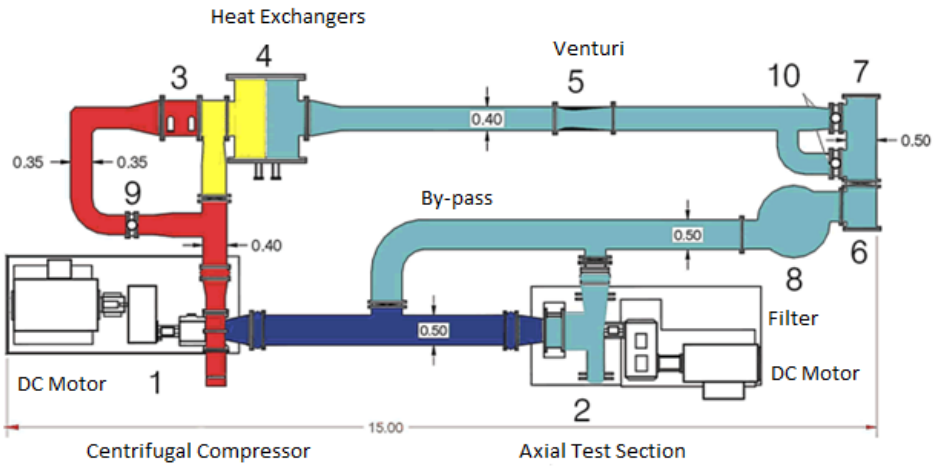

Figure 3.1 Schematic of the Test Rig [15]

The maximum power available at the centrifugal section is 800 kW while 400 kW are available at the axial one; the maximum rotational speed is 20000 Rpm for both the sections.

The two reversible DC engines allow a continuous rotational speed regulation and the electrical power generated at the turbine brake is reversed to the centrifugal section engine, leading to significant savings in electrical running costs.

Figure 3.2 Axial and Centrifugal Sections of the Test Rig

The test rig is instrumented in order to allow the over-all performance evaluation of both installed turbomachines. Both sections are equipped with traversing systems for the measurement of the flow field inside and downstream of the turbomachines; optical accesses for LDV measurements are also provided.

At the present time, the centrifugal section is equipped with a centrifugal compressor characterized by a nominal compression ratio of 2.2 at 6.5-7 kg/s (6.75 kg/s is fixed as the mass flow rate in CFD calculations) at a rotational speed of 18000 rpm, with the inlet at atmospheric condition (1 atm, 313 K).

3.1. Axial Flow Turbine Stage

The axial section is equipped with an axial turbine stage (Figure 3.3) representative of a modern HP stage characterized by a leaned stator and a bowed rotor rotating at 12000 Rpm; the casing(hub) diameter is 400mm and the blade height is 50 mm, thus the tip diameter has a value of 400mm.

The model of the HP gas turbine was designed for the purposes of the research program, PRIN 2003, concerning the analysis of unsteady effects in axial flow turbines. The design constraints led to a positive vane leaning of 12 degrees and to a significant blade bowing in the tip region. Table 1 reports the main geometrical characteristics and operational test condition of the turbine stage. The axial section was designed to allow different stator-rotor axial gaps by moving the stator row axially. The use of an unusually large maximum gap between the stator and the rotor (one stator axial chord) has been applied in order to mostly "switch off" the stator related flow effects downstream the stage. [16]

Figure 3.3 Axial Stage

	Vanes			Blades		
	Vane lean = 12 deg			Blade-passing freq. = 2.83 kHz		
Blades number	22			25		
Mean out. Mach	0.55			0.2		
Radial clearance (mm)	0.15			0.75		
b (mm)	30.6			46.7		
	Hub	**MS**	**Tip**	**Hub**	**MS**	**Tip**
S/*b*	1.39	1.6	1.86	0.80	0.94	1.07
Inletgeom. Angle (deg)		0		56.9	47.6	25.5
Outlet geom. Angle (deg)	72.5	75.2	77.5		−67.7	

Table 3.1 LFM axial flow turbine stage: Main geometrical and operational characteristics [16]

The rig doesn't contain a burning chamber and system works only with air on the turbine side which comes directly from the compressor instead of receiving exhaust gas. All CFD calculations are thus based on compressed air at 25 C degrees with a density of 2.32 kg/m^3; as the Mach number in the distributor (volute and IGVs) is always below 0.3 incompressible flow conditions have been considered.

The technical drawings of the test rig that were used as a base for the solid modeling of the volute are given in Appendix. Below there is the cross-section drawing of the volute of the centripetal turbine.

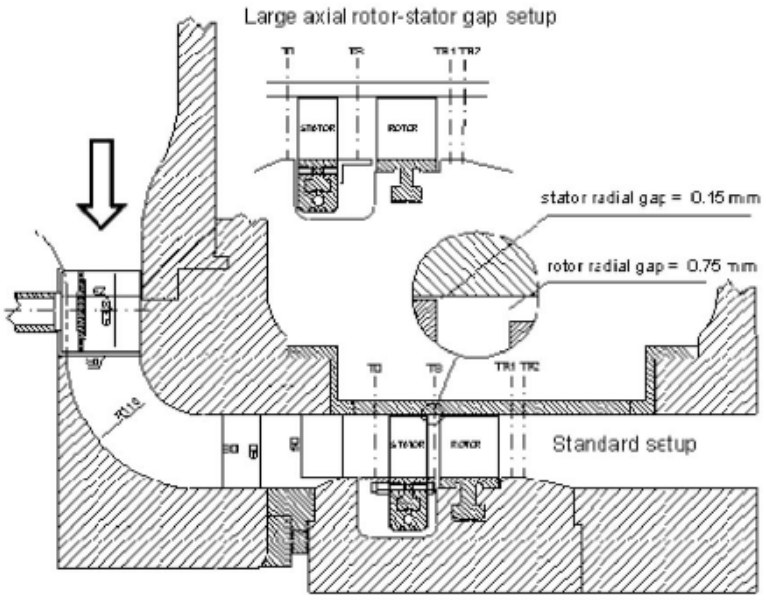

Figure 3.4 Sketch of the distributor

The inlet guide vanes that can be seen in the drawing are the original blades that were used in the machine and have an un-cambered profile that cannot fully provide axial and uniform flow at the inlet of the turbine. According to the results that have been derived from the simulations they will be replaced by new blades with a proper profile and geometry and experiments will be conducted for the verification of the simulation results.

Figure 3.5 Original Inlet Guide Vanes

The main purpose of the inlet guide vanes in this work is to reduce the blade-to-blade flow angle α, or the yaw angle, ultimately to zero at the inlet of the turbine stage. Since the distributor is centripetal the flow at the inlet section of the inlet guide vanes highly tangential (yaw angle of about 70 degrees). As the original blades are inefficient in turning flow from tangential to axial direction a new design is required.

Chapter 4

Preliminary Analysis of the Volute and the Determination of the Flow Characteristic

This chapter will be devoted to the process of the solid modeling of the centripetal flow distributor, or the volute, of the axial turbine that the work and the CFD simulations are based on and the determination of the flow characteristics inside the volute by a CFD analysis where the flow is simulated without the presence of IGVs.

4.1. Design of the Flow Region inside the Volute

The initial design was solely based on the original technical drawings which are presented in the Appendix. Later on the design was modified several times considering the changes in the real volute and the turbine. Several mechanical measurements were made on the dismantled turbine for the points in the drawings that weren't clearly apparent.

Below, four different views of the final drawing of the flow region in the volute can be seen after a number of changes in the geometry.

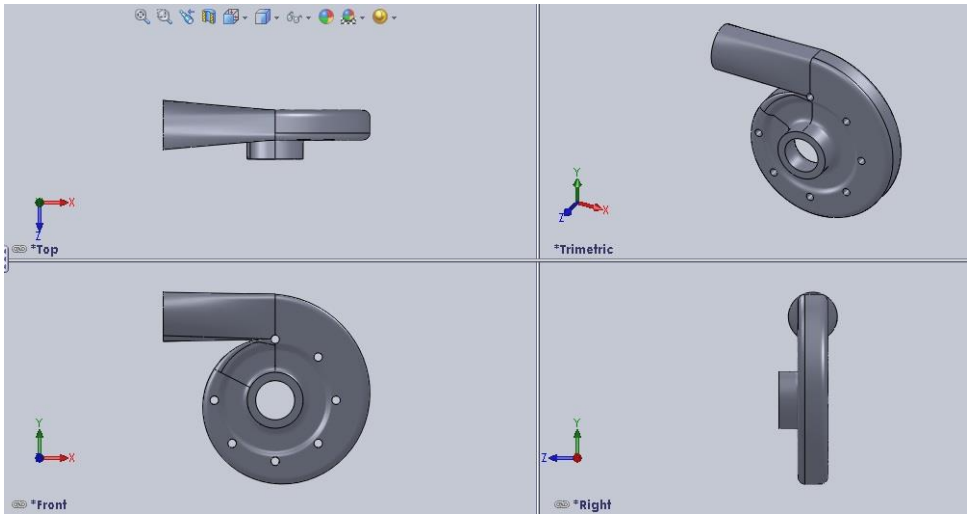

Figure 4.1 Four different views of the final design

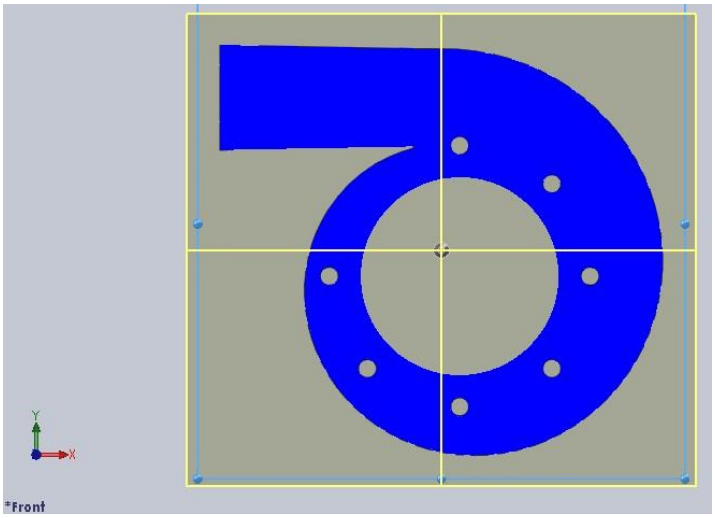

Figure 4.2 Cross-section of the volute

It should be noted that some of the required dimensions and values do not exist in the technical drawings that are presented in the Appendix and they should be presented here. The length of inlet channel to the volute is 800 mm starting from the flange with an internal diameter of 350 mm that could be seen in the technical drawings ending at the first stiffener. The holes that can be seen in the cross-sectional view are the stiffeners. They are placed once in every 45 degrees except the last one at 315 degrees numbering seven. These stiffeners are used to give the required strength to the machine although at the same time they generate separations in flow downstream. The volute (Figure 4.2) has a spiral shape which allows a stable fluid flow through the channel. The spiral is developed according to the technical drawings which indicate that the radius of the volute decreases 8 mm at every 9 degrees; as a result the spiral ends at the center point of the first stiffener at when we reach 360 degrees. The inlet channel has a circular entrance while the exit of the channel has a rectangular shape allowing to the flow a smooth transition into the volute.

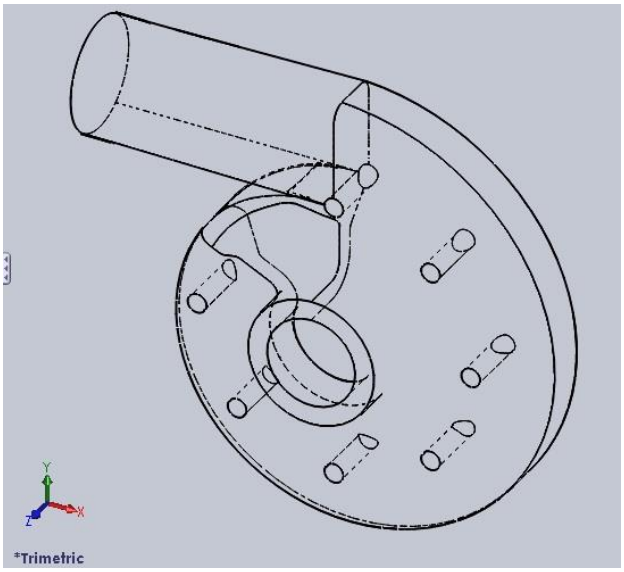

Figure 4.3 Detailed view

One important point in the design of the volute was the modeling of the tongue between the main centripetal part of the distributor and the inlet channel. The purpose of the tongue is to create an adequate space and a smoother transition area to prevent flow detachment just as the flow enters the main distributor channel exiting the inlet channel, thus reducing the losses through the flow. The main problem with the design of the tongue was that this structure was non-existent in the technical drawings but due to practical reasons that have been mentioned above it exists in the test rig and its design in the solid modeling software is solely based on observation and measurements made on the actual machine. The measured data for the design of the tongue indicates that the external distance between the flange and the tongue is 420 mm. The internal distance between the flange and the tongue is 650 mm and the tongue has a radius of more or less 15 mm. According to these data a tongue that would be most close to the real case was modeled as it can be seen in the Figure 4.4.

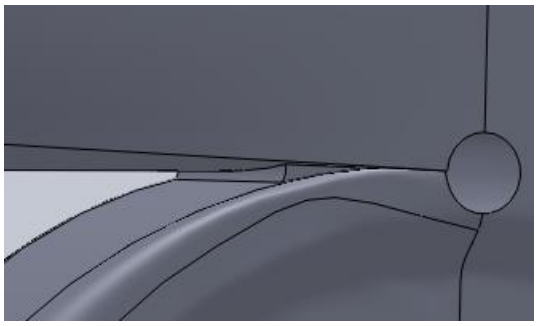

Figure 4.4 The tongue

The last point that should be mentioned about the preliminary design is that during the process it was discovered that the distributor was manufactured very differently in the lower part of the channel (near the inlet of the axial turbine). There were several sections with geometrical irregularities. The channel was not circular and dimensions were different as compared to the technical drawings to an extent that cannot be neglected. Real dimensions were determined from the Figure 4.5 by using SketchUp 8, a 3D modeling program which allows importing files in pdf format, such as performed in the present study.

The preliminary design was already completed when this issue of geometric irregularity was realized and the solid model of the flow region was not changed further, as the flow characteristics were determined for the inlet of the IGVs based on the pre-determined inlet and outlet conditions for the volute and the effect of the difference between the drawings and the real case on upstream flow conditions can be neglected. However, as it will be mentioned in the next chapter the deviation in the geometry significantly affects the flow conditions at the outlet section of the volute (inlet of the axial turbine) as it is presently the upstream of the region that is investigated and this issue was addressed in the CFD simulations of the IGVs.

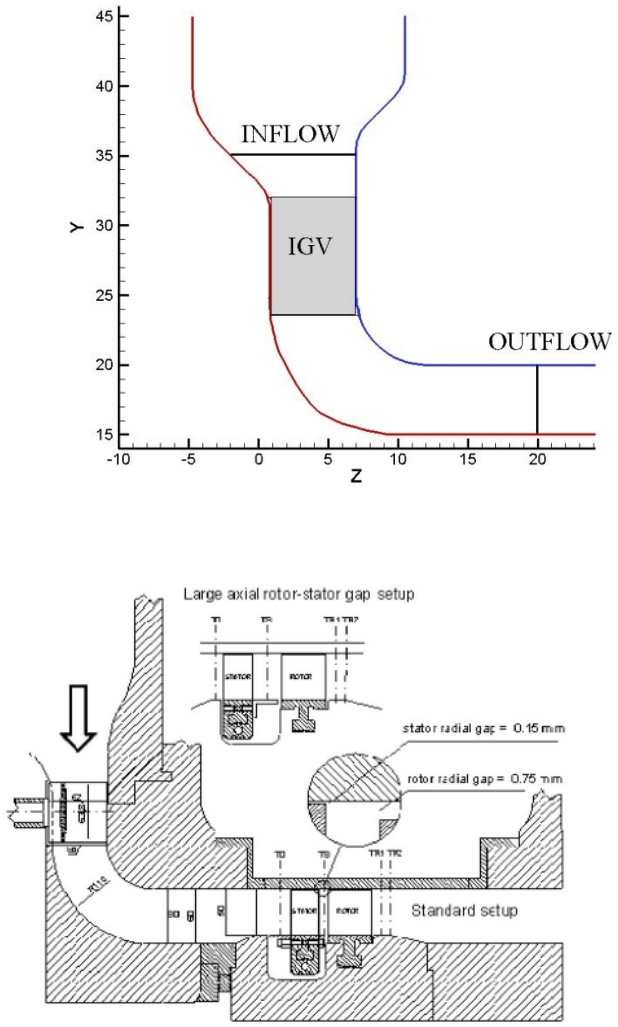

Figure 4.5 Real and theoretical cross-sections of the centripetal distributor

4.2. Determination of the Flow Characteristics

After the finalization of the design of the volute, a CFD simulation of the flow region without any blade was accomplished by using a mesh generator software (Flowizard) and a viscous flow solver (ANSYS-Fluent) to analyze the results. The flow solver used in this context shares most of its computational and modeling features with ANSYS-CFX, the solver used for the detailed IGV design.

The analysis was made in order to determine the flow characteristics at the inlet of the IGVs (r=0.325 m) which were required for the subsequent part of this work which contains the optimization of the IGVs in order to get a full axial flow at the inlet of the axial turbine.

4.2.1. The Mesh

The initial simulation by using the geometry created in the previous steps is imported to Flowizard, an automated meshing software that allows an easy way of mesh generation by describing the geometry, fluid and flow properties, boundary conditions and by a choice between calculation speed versus accuracy.

The geometry of the flow region was defined as symmetric and the unit of length is taken as mm. The flow type was defined as turbulent and the working fluid, which is air, as incompressible with no rotating machinery inside the calculation domain.

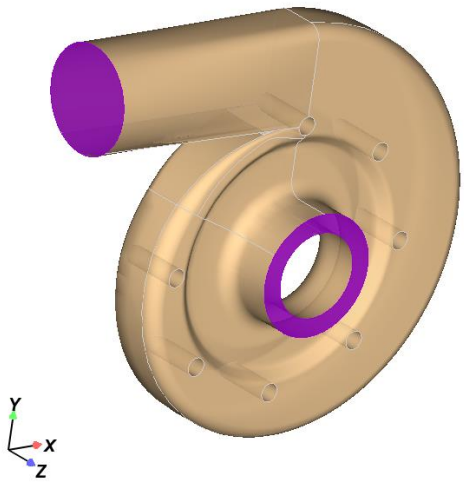

Figure 4.6 Inlet and outlet

Three separate surface groups with different boundary conditions were specified.

1. **Stationary Walls:**
   No Flow
   Insulated (adiabatic) wall

2. **Inlet:**
   Total pressure: 225000 Pascal
   Flow normal to inlet
   Source of flow: long tube, pipe or duct
   Temperature at inlet : 330 C
3. **Outlet:**
   Pressure: 215000 Pascal

Increased accuracy near walls, in simple geometries and small gaps were specified during the process while critical length and angle were determined as 4.94 and 20, respectively, which results in smaller lengths and angles being eliminated during the calculation. In the end of the process maximum accuracy over speed was preferred, as accuracy at this stage was more important than the speed due to the fact that the flow characteristics derived at this stage would affect the later stages of the whole work. Furthermore, this calculation is not routinely performed in the design phase so the computational time of this single calculation has a limited impact on the overall design process. Below, the complete mesh generated at the end of this process can be seen, which is a tetrahedral mesh composed of 1031340 cells.

Figure 4.7 The Mesh

4.2.2. Simulation on Fluent

After the finalization of the mesh of the whole volute with the correct boundary conditions the simulation was carried out on Fluent. In Figure 4.8 static pressure distribution throughout the volute can be seen.

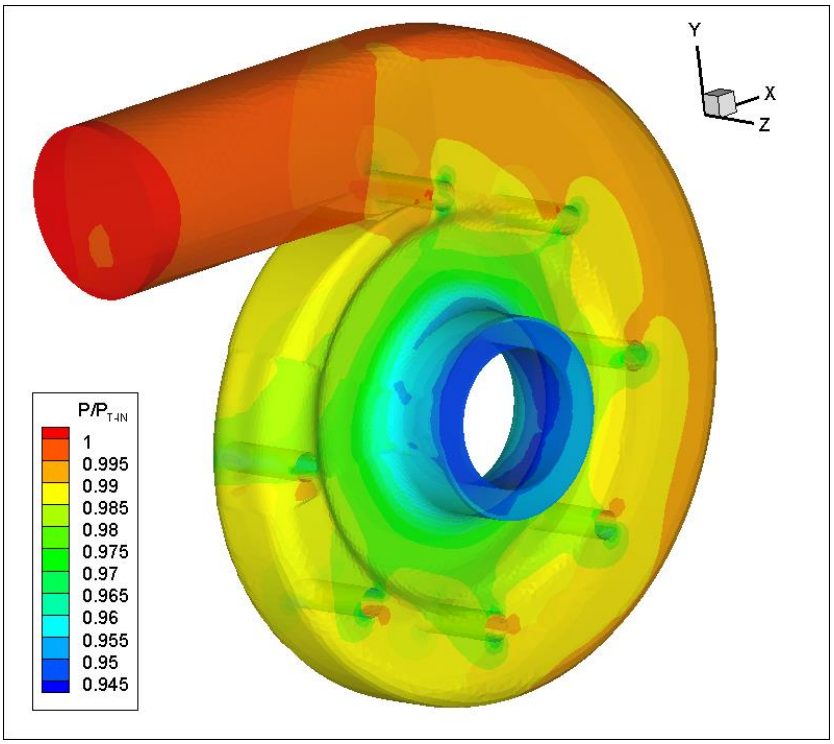

Figure 4.8 Static pressure distribution

The results obtained from the simulation were used as a base for the further simulations done with the IGV inside the volute. As a first step the data set for a cylindrical section defined on the radius of 0.35 m were obtained; this position represents the position of the inflow boundary for the subsequent CFD modeling of the IGVs. The data were composed of the values of the relevant coordinates for each point, then pressure, total pressure and velocity components on x, y and z axes on the 20 spanwise positions, with 1 degree resolution in circumferential direction resulting in 7200 values for each of the mentioned flow properties. In Figures 4.9 and 4.10 distributions of total pressure and yaw angle for the cylindrical surface created for the specified radius can be seen.

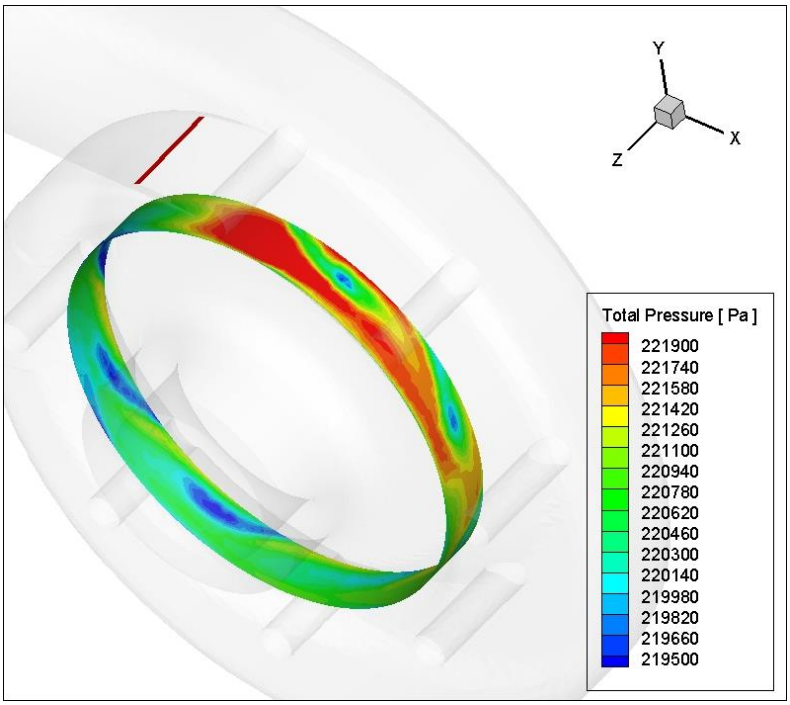

Figure 4.9 Total pressure distribution at cylindrical section of radius 0.35 m

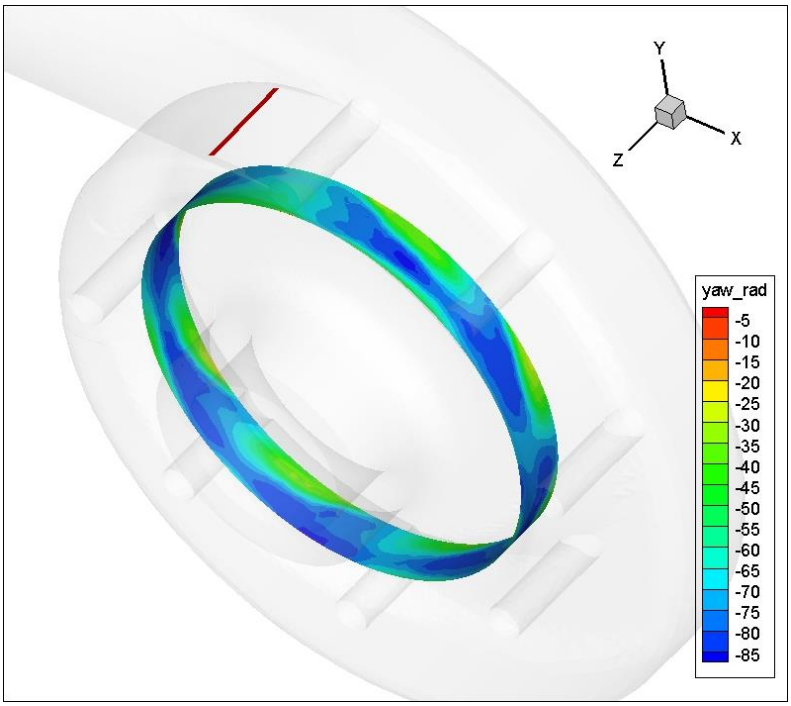

Figure 4.10 Yaw angle distribution at cylindrical section of radius 0.35 m

As the second step a code in Fortran (which is presented in the Appendix) was written to integrate the values obtained from the simulation on Fluent over the loop for 360 degrees for each spanwise position, aiming to get pitchwise averaged values for pressure, total pressure, axial, tangential, radial velocities, yaw and pitch angles for each of the 20 spanwise positions. Below, the formulas utilized in the Fortran code are presented for the mean values;

Area of the element of cylindrical surfaceat specified radius:

$$S = \int_0^h \int_0^{2\pi} r d\theta dl = h \int_0^{2\pi} r d\theta \tag{4.1}$$

G , mass flow:

$$G = \int_S \rho V_{rad} dS = \int_0^h \int_0^{2\pi} \rho V_{rad} r d\theta dl \tag{4.2}$$

which can be rewritten as,

$$= \rho h \int_0^{2\pi} V_{rad} r d\theta \tag{4.3}$$

where h is the total length of the element of cylindrical surface in z axis.

For the axial, tangential radial velocities and the total pressure a general formulation can be written in the form of,

$$\overline{\Psi} = \frac{\int_S \rho \Psi V_{rad} dS}{G} = \frac{\int_0^h \int_0^{2\pi} \rho \Psi V_{rad} dS}{\rho h \int_0^{2\pi} V_{rad} r d\theta} \tag{4.4}$$

as ρ is assumed to be constant and taken out of the integral ultimately we can write,

$$\overline{\Psi} = \frac{\int_0^{2\pi} \Psi V_{rad} r d\theta}{\int_0^{2\pi} V_{rad} r d\theta} \tag{4.5}$$

where Ψ is a representative symbol for V_{rad}, V_{tg}, V_{ax} and P_t, thus putting V_{rad} instead of Ψ into the formula by also considering that r is constant, we can obtain the formula for radial velocity;

$$\bar{V}_{rad} = \frac{\int_S V_{rad}^2 dS}{\dot{V}} \tag{4.6}$$

Similarly obtained formulas for other properties are,

$$\bar{V}_{tg} = \frac{\int_S V_{rad} V_{tg} dS}{\dot{V}} \tag{4.7}$$

$$\bar{V}_{ax} = \frac{\int_S V_{rad} V_{ax} dS}{\dot{V}} \tag{4.8}$$

$$\bar{P}_t = \frac{\int_S V_{rad} P_t dS}{\dot{V}} \tag{4.9}$$

Meanwhile other formulas for the flow properties that are used are:

Pressure:

$$\bar{P} = \frac{\int_S P dS}{S} = \frac{\int_0^h \int_0^{2\pi} P\, r d\theta dl}{\int_0^h \int_0^{2\pi} r d\theta dl} \tag{4.10}$$

which is subsequently equal to

$$\bar{P} = \frac{\int_0^{2\pi} P r d\theta}{2\pi r} \tag{4.11}$$

Blade to blade velocity:

$$\bar{V}_{bl-to-bl} = \sqrt{\bar{V}_{tg}{}^2 + \bar{V}_{rad}{}^2} \tag{4.12}$$

Yaw angle:

$$Yaw_{rad} = arctg\left(\frac{\bar{V}_{tg}}{\bar{V}_{rad}}\right) \tag{4.13}$$

Pitch angle:

$$Pitch_{rad} = arctg\left(\frac{\bar{V}_{ax}}{\bar{V}_{bl-to-bl}}\right) \quad (4.14)$$

For the final step to determine the flow characteristics as the inlet conditions of the IGV simulations, these 20 sets of data for the flow properties were further averaged along the span to get a single value for each of them on the whole cylindrical surface at the radius of 0.35 m. The obtained values for the overall averages for pressure, total pressure, radial velocity, tangential velocity, axial velocity, yaw angle and pitch angle at 0.35 m radius are;

- Pressure: 218327.70 Pascal
- Total Pressure: 220826.07 Pascal
- Radial Velocity: -17.98 m/s
- Tangential Velocity: 37.65 m/s
- Axial Velocity: 9.81 m/s
- Yaw Angle: 64.46 degrees
- Pitch Angle: 13.23 degrees

These values are used as the input data for the simulations in the next step of this work, from where the ultimate yaw angle at the inlet of the axial machine would be derived. As it can be observed from the Figure 4.11 the yaw angle at the distributor, upstream of the inlet guide vanes have a very high value with a mean value equal to 64.4636 degrees which definitely needs to be reduced at the end of the channel.

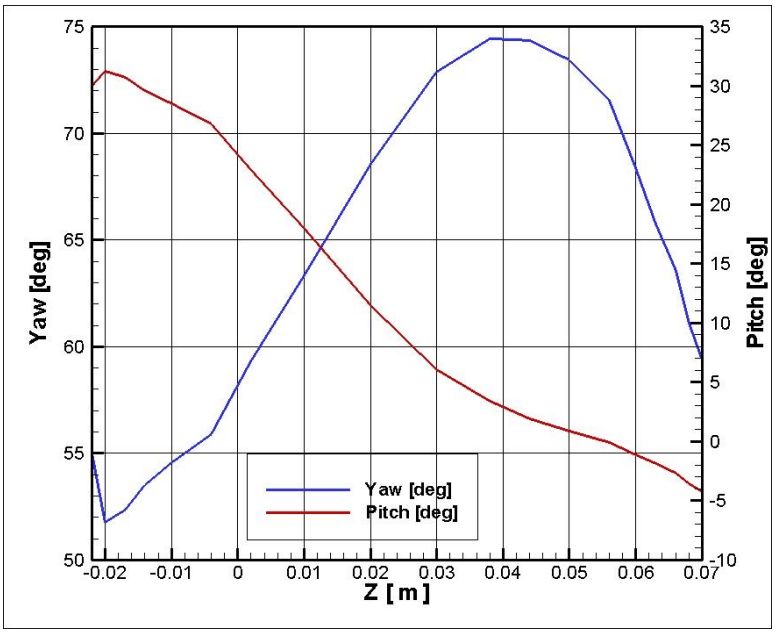

Figure 4.11 Spanwise Distribution of pitchwise-averaged Yaw and Pitch Angles

Chapter 5

Optimization of the Inlet Guide Vane Profile and Results

The CFD simulation that has been conducted until now was aimed at simulating the whole flow region of the volute model without any inlet guide vanes present in the structure. The present chapter of this work is dedicated to the several CFD simulations of the flow channel with inlet guide vanes of different configurations, profile types and number of blade sets. A description of the computational domain and mesh generation process will be described as this part of the simulation remains mostly unchanged throughout the process of examining different profiles along with the description of the boundary conditions which have been already discussed in the end of the Chapter 4. A comparative table with the results of the simulations for each different configuration is presented at the last part of the chapter. Some of the important and critical simulations and design choices will be commented on in detail.

The final aim of these simulations is to develop a solution to the problem of obtaining fully axial flow (or yaw angle equal to zero) at the exit of the channel. The solution is expected to be with an appropriate and applicable blade profile considering the constraints imposed by the whole distributor system.

5.1. Computational domain and Mesh

The first point that should be mentioned is that the computational domain discussed in this section does not cover the whole flow region but just the blade channel. This action is taken in order to decrease the heavy computational burden on hardware because for the IGV simulations the resolution of the grid is increased greatly due to the fact that the desired accuracy is increased according to the detailed requirements of this study. The whole flow region in the volute is accordingly divided into 30 blade channels for the given configuration with 30 IGVs (or in the case of 60 blade-configuration, 60 blade channels) based on the fact that the geometry and the

flow conditions assures the periodicity conditions between each blade of the IGV cascade.

The mesh of the computational domain was developed and generated by Turbogrid, a module of ANSYS CFX using curve files to create the geometry. Below, in the Figure 5.1the computational domain can be seen starting from the radius of 0.35 meters ending at the inlet of the blades of the axial turbine. The domain in the Figure 5.1 represents the configuration with 30 blade sets for one of the profiles that were tested.

The blades were positioned by taking the yaw angle at 0.35 m radius into account. As the yaw angle at 0.35m is 64.5 degrees, with a significant part of the channel (at the hub endwall) characterized by significantly lower flow angles, an angle of 60 degrees was assigned at the leading edge as best compromise for the whole blade span; as the trailing edge is positioned radially at about 0 degrees, the difference between the leading and the tailing edges is about 60 degrees. In the final stages of the work this difference was increased by turning the tailing edge. These data further clarify the severe limitations imposed by the use, in the original IGVs, of un-cambered profiles.

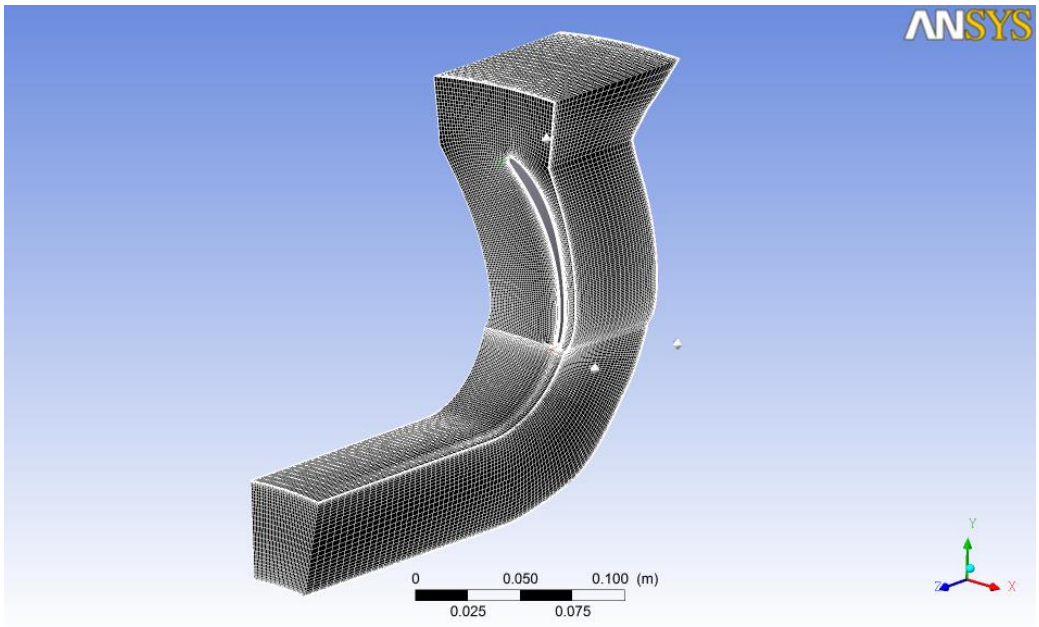

Figure 5.1 The computational domain

During the meshing process, an approach for the highest possible accuracy was chosen. Node count target was specified as 500000 for achieving a grid with a fine structure. Boundary layer refinement control method was chosen so as to be proportional to mesh size. The y^+ method was used for the near wall element size specification; most part of the simulations were performed with y^+ at the blade walls.

For the passage, namely the flow channel around the blade that can be seen in the Figure 5.2, the boundary layer cell structures for each of the hub, the shroud and the area between them were specified. For the hub, and for the shroud which is structured in the same way, the layer offset is chosen as 0.1, meaning that 10% of the total passage is treated as the boundary layer. Finer cells are considered for the boundary layer zone. Element count and size were specified for the hub and the shroud with number of elements equal to 10 and y^+ equal to 50 (the value of y^+ was kept as 50 in the initial simulations, for the final simulations, as the work needed a higher accuracy the y^+ value was decreased to 1). The area between the boundary layers was fixed to have 20 elements as this area needs a lower amount of cells for the computation.

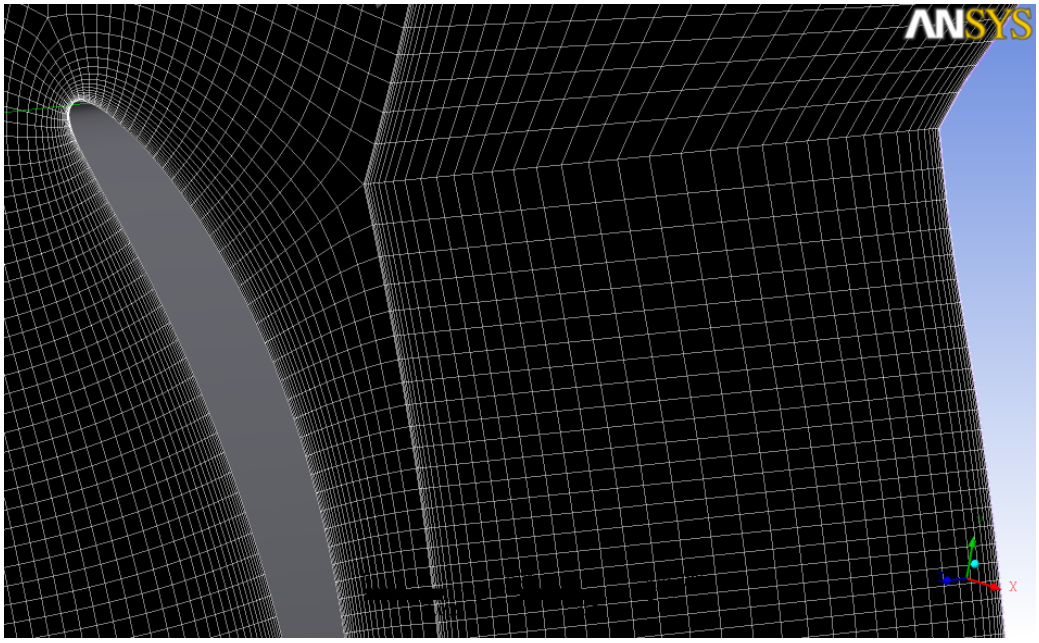

Figure 5.2 The detailed view of the cells in the boundary layers

For each computational case, the estimated value of y^+ was compared with the real value in the boundary layer next to wall to check the quality and the reliability of the generated mesh.

Mesh type was chosen as H-grid at the inlet, outlet and throughout the flow channel. The limits of the generated mesh were specified such that the maximum and minimum face angles were 165 and 15 degrees.

5.2. Boundary Conditions

After the generation of mesh, boundary conditions on the computational domain were imposed. ANSYS CFX-Pre was used as a pre-processor to introduce the simulation characteristics and boundary conditions to the meshed structure.

For the basic settings characterizing the flow, the blade channel was identified as a radial distributor with a single, fixed blade row which was the most similar case to the volute structure that had to be simulated. Domain reference pressure was identified as 0 Pascal and the steady state solution is considered.

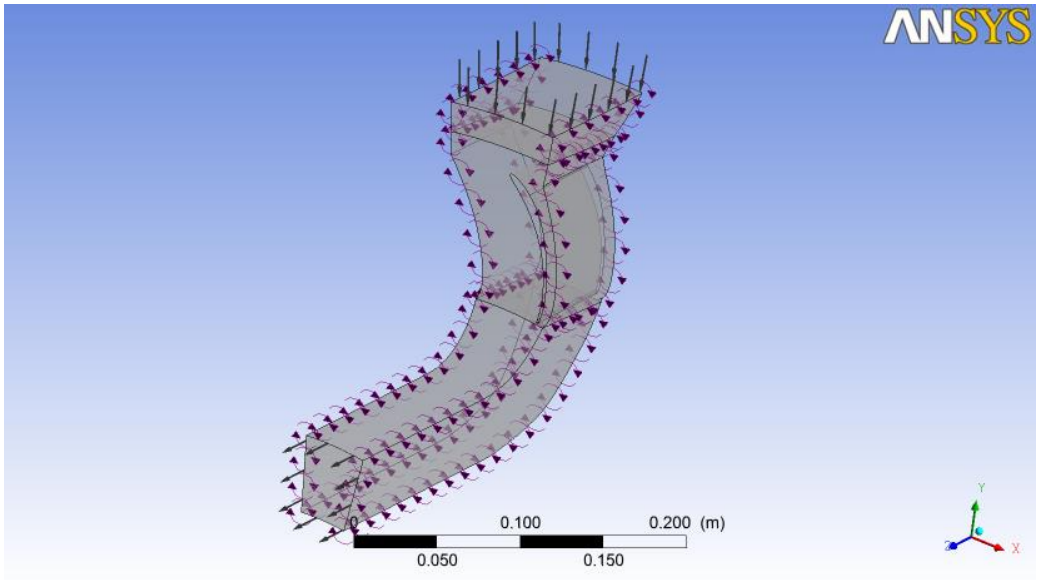

Figure 5.3 Flow Channel in pre-processing stage

As a second step the physics of the flow was defined. Fluid inside the channel is identified as air at 25 C with a density of 2.32 kg/m^3. Although there is no increase in temperature, the effect of high pressure must be taken into account. It was also assumed that there is no heat transfer in the computational domain.

At the inlet of the domain, velocity profile and the total pressure was introduced as the boundary conditions. In Figure 5.4 it can be observed that inlet section of the flow channel is sloped in the hub and this creates problems for the solution when an average velocity in y direction is introduced for the boundary conditions. Assigning a uniform radial-inflow velocity profile to the inlet means that the flow directly encounters a sloped surface at the hub and this situation creates distortion in the flow that is non-existent in reality.

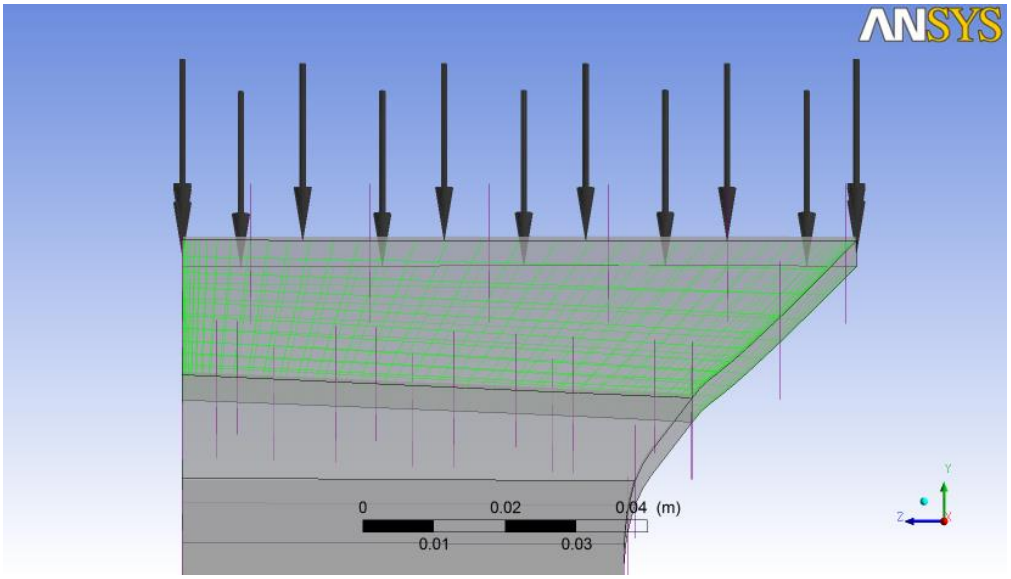

Figure 5.4 Sloped inlet section

To overcome this problem, the components of velocity profile at the inlet were assigned separately. In Figure 5.5, a detailed view is presented.

As we need another boundary condition in the inlet, the total pressure is given as 220826.07 Pascal, based on the results that were obtained in the previous chapter. The outlet static pressure although assigned initially as 215000 Pascal is changed throughout the process in the solver so that the mass flow at the outlet of the blade channel stays the same as 0.225 kg/s for the 30-

blade configuration (thus the total mass flow at the outlet is 0.225x30 = 6.75 kg/s). For the 60-blade configurations the total pressure at the outlet is considered in such a way that the mass flow at the outlet of the channel is 0.1125 kg/s. It should be noted that in this problem the well-posedness is not compromised by assigning the mass flow at the outlet, as no choking conditions could occur. The flow regime both at the inlet and outlet is also defined as subsonic (and incompressible) and the turbulence intensity was specified as %5 (medium).

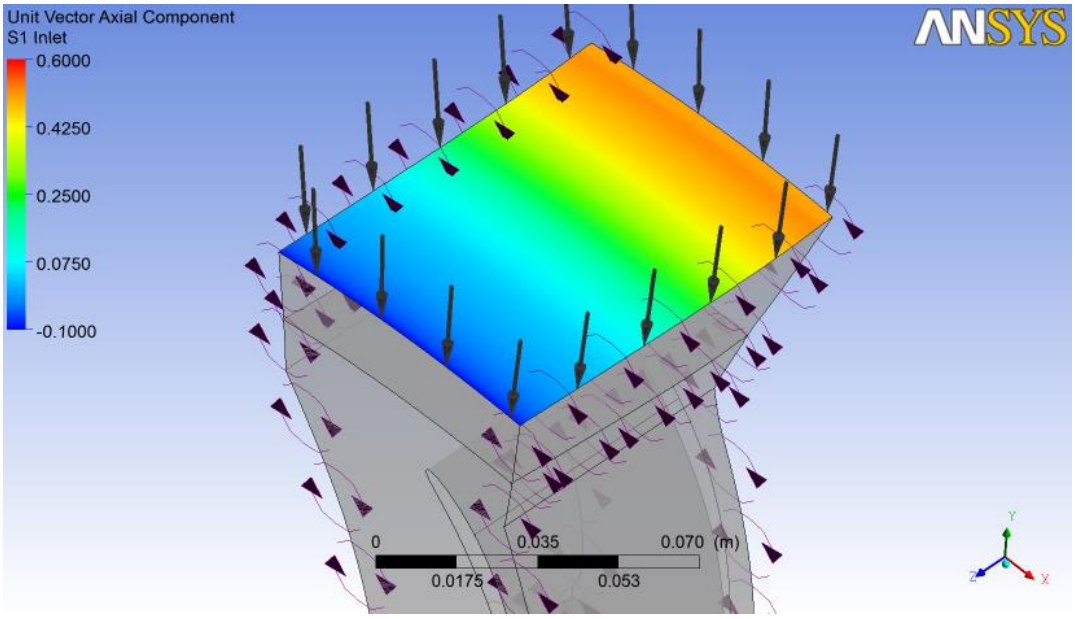

Figure 5.5 Detailed view of the inlet conditions

Boundaries of the computational domain were specified as wall surface with no slip at the hub, at the shroud and at the blade while the wall was assumed to be smooth neglecting the roughness that may exist in the real machine.

Turbulence model was chosen as Shear Stress Transport model. The Shear Stress Transport model, or shortly SST k-ω turbulence model is a two-equation eddy-viscosity model which is very popular for commercial products as it combines the best part of two different models. In In SST k-ω model, k-ω formulation is used in the inner parts of the boundary layer which makes the model directly applicable all the way down to the wall through the viscous sub-

layer. Thus the SST k-ω model can be used as a Low-Re turbulence model without any extra damping functions. The SST formulation also switches to k-ε behavior in the free-stream, thus overcomes the common k-ω problem that the model is too sensitive to the inlet free-stream turbulence properties. The SST k-ω model has advantages in predicting in adverse pressure gradients and separating flow. This is a crucial feature for the present problem, in which local separations are expected. The disadvantage of the SST k-ω model is that it produces large turbulence levels in some regions like stagnation regions and regions with strong acceleration although this effect is much weaker than with a normal k-ε model.[17,18]

Wall functions were chosen to be automatically used (at the endwalls, where the grid refinement is not significant as it is at the blade surface), while also at the same time mesh correction on periodic surfaces is also automated.

Solver controls in this stage were adjusted in such a way that both the advection scheme and turbulence numeric would have a high resolution.

As the solution (in terms of computation time and storage) would be really a heavy burden, or even impossible on a personal computer the solver module CFX-Solver Manager was run on the cluster of Politecnico di Milano.

5.3. Data Reduction of the Solution

At the final stage of the simulation, the results obtained are analyzed in the post-processor, CFD-Post. The results of all of the simulations that have been performed are presented in Table 5.1 in the Results section.

The main parameters obtained from the solution are the pressure, total pressure, velocity, velocity components in axial, circumferential and radial directions, velocity flow angle (yaw angle) and total pressure loss coefficient for the two surfaces that can be observed in Figure 5.6. One of the surfaces is created just at the inlet of the blades (for shorter blades this surface was created at r = 0.32 m while for the configurations with longer blades the surface was at r= 0.325 m). The other one that is used to extract the final results is created at the outflow at the computational domain.

Besides these main parameters in order to analyzethe characteristics of the flow, several images of the streamlines, total pressure distribution which

indicate the flow separation around the blades and the losses at several spanwise positions were obtained. Also radial velocity was inspected at the outlet of the domain to observe the existence of vortices in the turbine inlet.

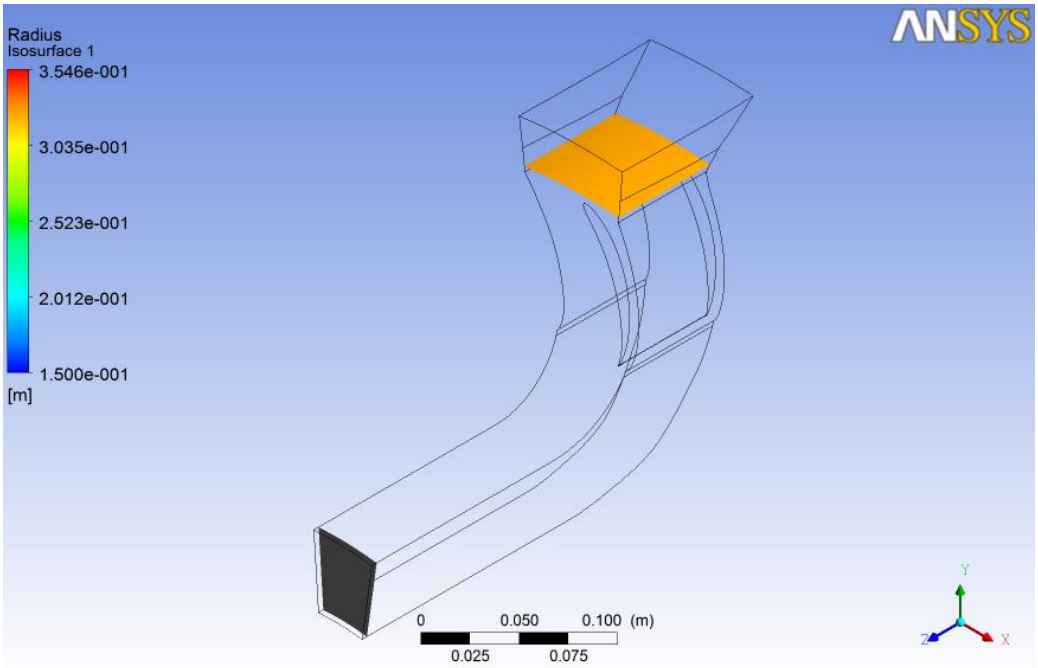

Figure 5.6 The surfaces used for the analysis of the solution

The total pressure loss was calculated according to the equation below;

$$Y = \frac{P_{T1} - P_{T2}}{P_{T1} - P_2} \tag{5.1}$$

where the indices of 1 and 2 indicate the surface at the inlet of the blades and the outlet of the computational domain respectively.

5.4. Critical Changes in Blade Geometry and Significant Simulations

5.4.1. Original Inlet Guide Vanes

Original Inlet Guide Vanes used in the volute have a profile geometry similar to NACA0012 with a length of 64 mm. The original blades were used first in the simulation to have an idea on the initial situation of the volute to be compared with the newer blade designs.

The original IGV were used in two different configurations depending on the geometric angle of the edges, either +15 degrees or -15 degrees. The results obtained from the solutions show that there is a very high residual flow angle with an average value of 20.82 and – 20.99 degrees, respectively for the cases of +15 and -15 degrees, in the outlet of the computational domain which can also be observed from the Figure 5.7 and Figure 5.8 below (Charts obtained from CFX-Post evaluate the flow angle with an addition of 90 degrees, so the flow angle is 110 degrees in the chart below).

Also in the original IGVs it was seen that there is a really high pressure loss, possibly due to the positioning of the blades and flow separation caused by the positioning as well which can be observed in Figure 5.9 and Figure 5.10. The total pressure loss coefficient was found to be 17.17 % and 33.4 %, respectively for the cases of +15 and -15 degrees.

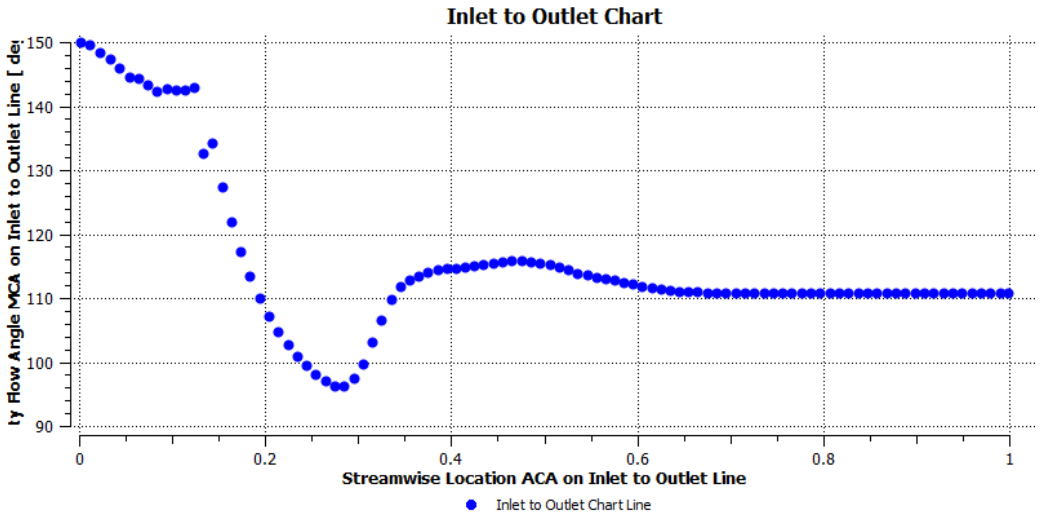

Figure 5.7 Streamwise Flow Angle Chart (Original IGV, +15 degrees)

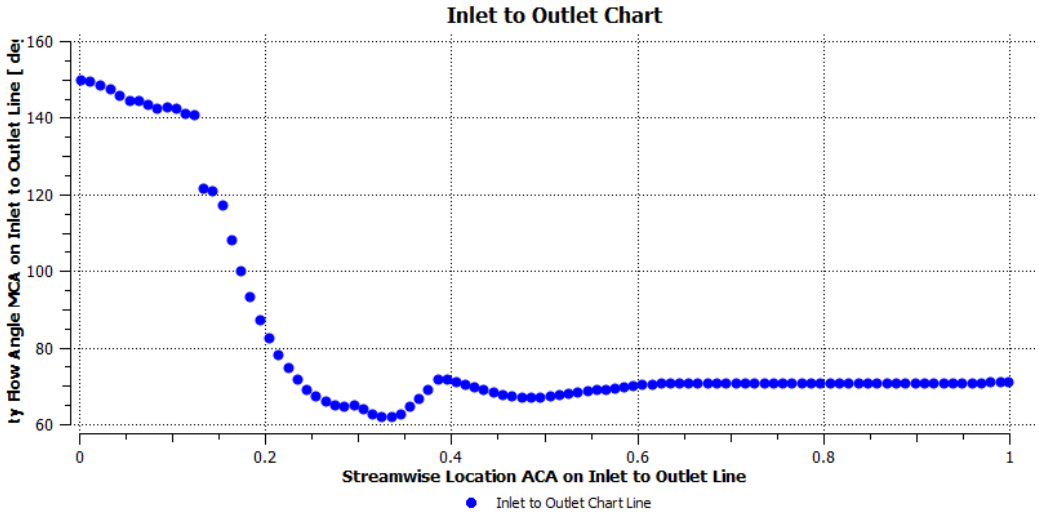

Figure 5.8 Streamwise Flow Angle Chart (Original IGV, -15 degrees)

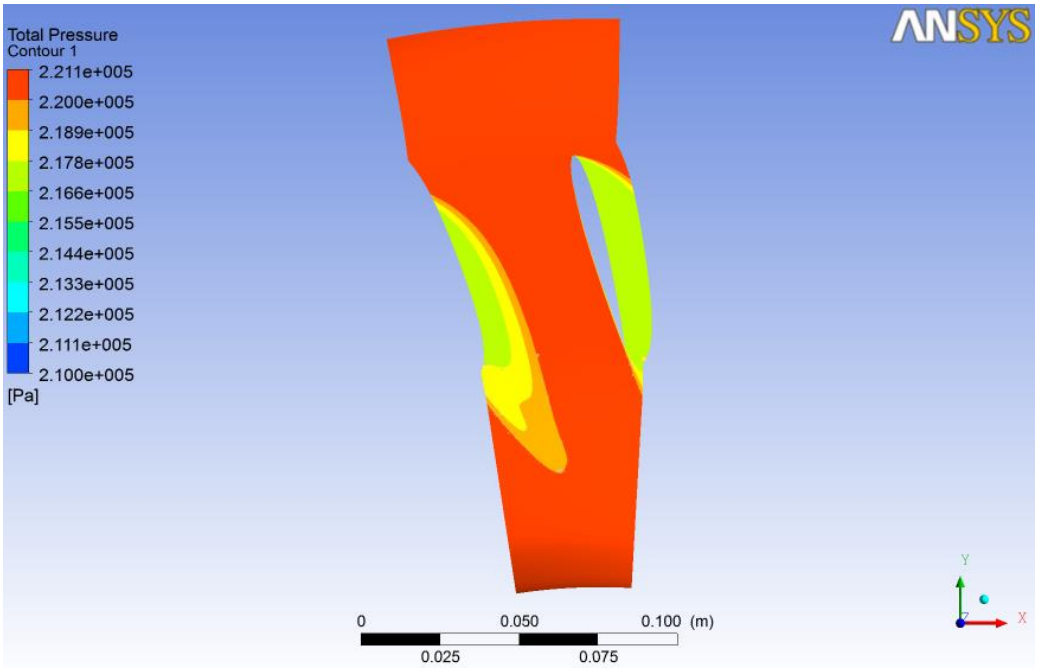

Figure 5.9 Total Pressure Distribution at midspan (Original IGV, Trailing Edge at +15 degrees)

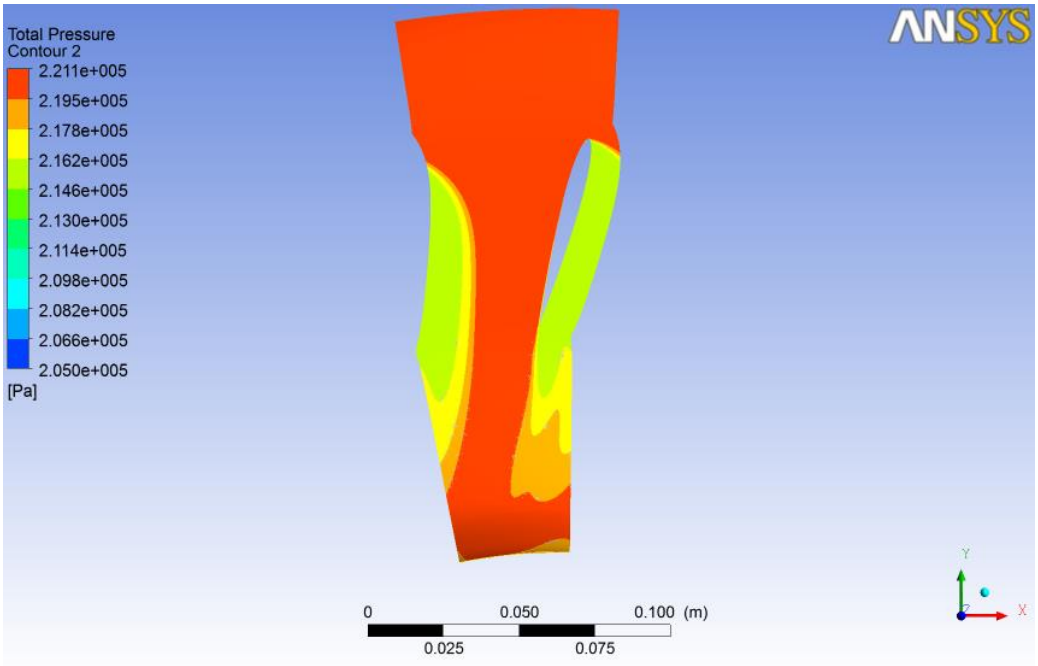

Figure 5.10 Total Pressure Distribution at midspan (Original IGV, Trailing Edge at -15 degrees)

5.4.2. Circular Arc Mean Line (CAML) with 30 and 60 Blades

Instead of an NACA profile, a circular profile was tested in one of the initial simulations. The main motivation in testing a curved profile type unlike an un-cambered NACA profile is to match the inlet and outlet flow angles at the leading and trailing edges of the blade with the geometric angles of the blade while the regulation in flow angle is not required once a certain profile geometry fulfills the requirements for the flow direction. The results obtained from the solution show that there is still a high residual flow angle in the outlet of the turbine, although it is decreased compared to the original blades. For the configurations with 30 and 60 blades, the values of flow angles were 13.69 and 9.68 degrees, respectively. While the flow angle is lower for the configuration with 60 blades, the total pressure loss is 17.67% which is much higher compared to 7.95% in case of 30 blades. The flow angle charts for both cases are presented below.

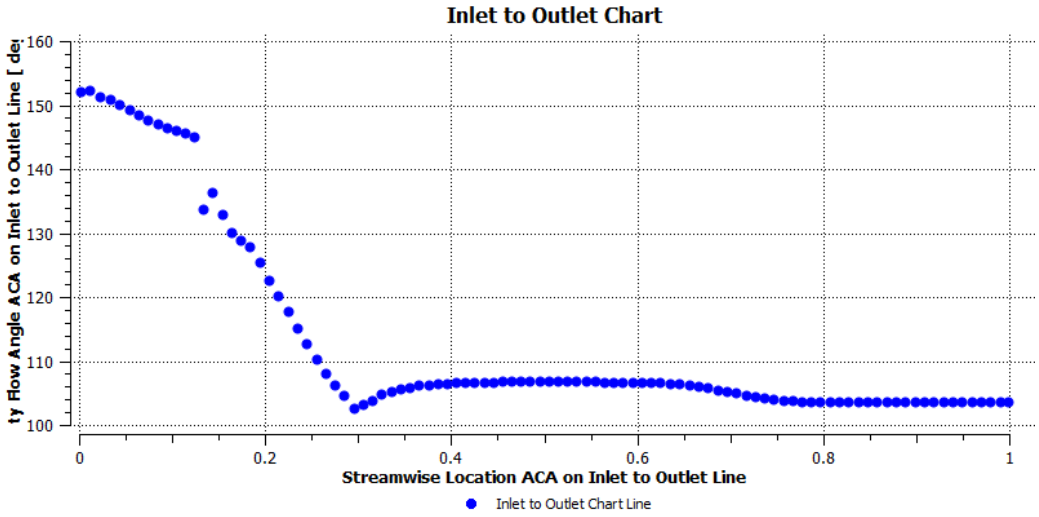

Figure 5.11 Streamwise Flow Angle Chart – 30 Blades (CAML)

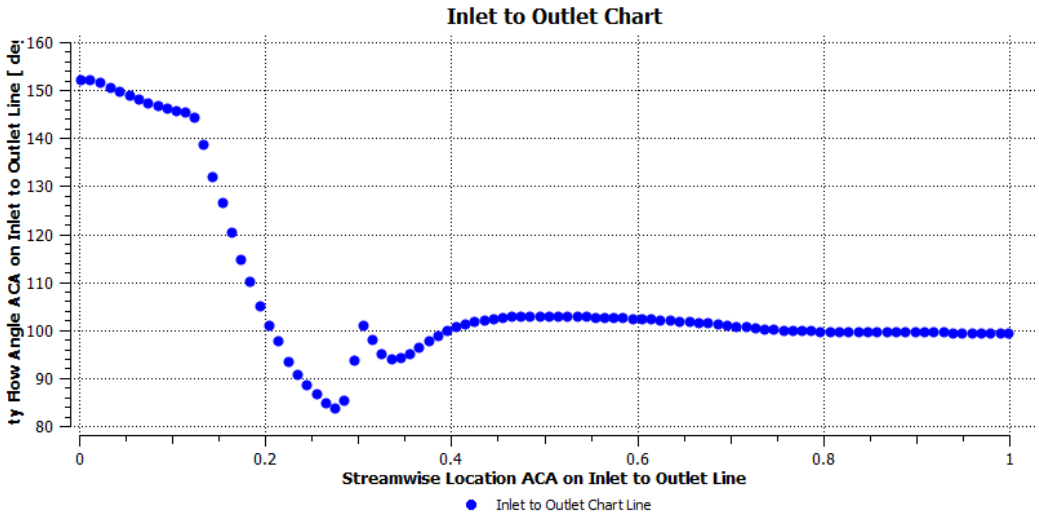

Figure 5.12 Streamwise Flow Angle Chart – 60 Blades (CAML)

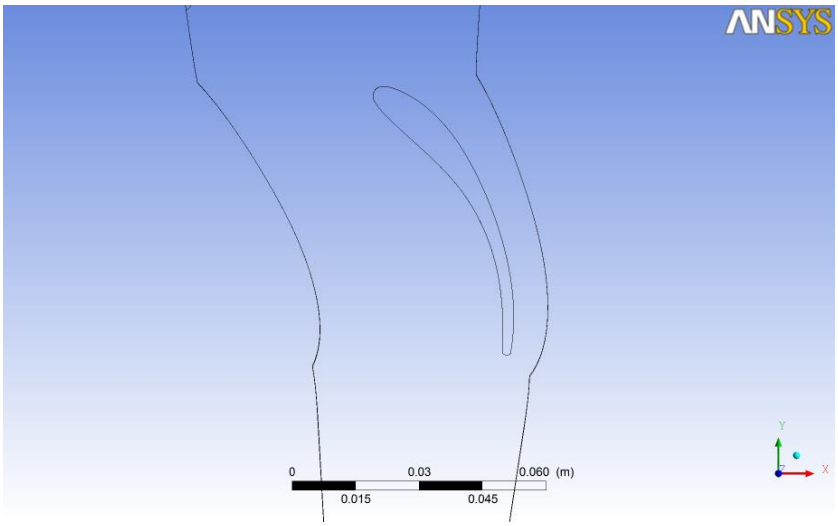

Figure 5.13 Profile View of the CAML Blade (30-Blade Configuration)

5.4.3. Elliptic Arc Mean Line (EAML) of Ellipse Factor 2 with 30 Blades

As the CAML blade was not considered efficient enough to achieve a good result the blade mean line was changed to elliptic mean line. Ellipse Factor 2 means that the axis of the ellipse in azimuthal direction is the double of that in the radial direction. The flow angle and total pressure loss obtained from the solution in 30 blade configuration are 18.14 degrees and 9.78%, respectively, showing clearly that the ellipse performs in a worse way with respect to the circle; this is due to the sever curvature of the blade mean line in the rear part. The further attempt was made developing a profile with elliptic mean line in the

opposite direction.

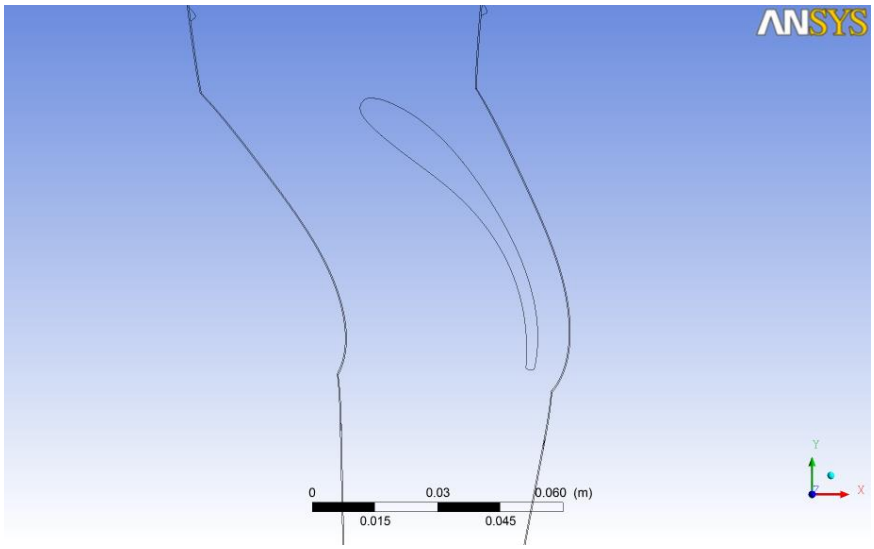

Figure 5.14 Profile View of the EAML Blade with an Ellipse Factor = 2 (30-Blade Configuration)

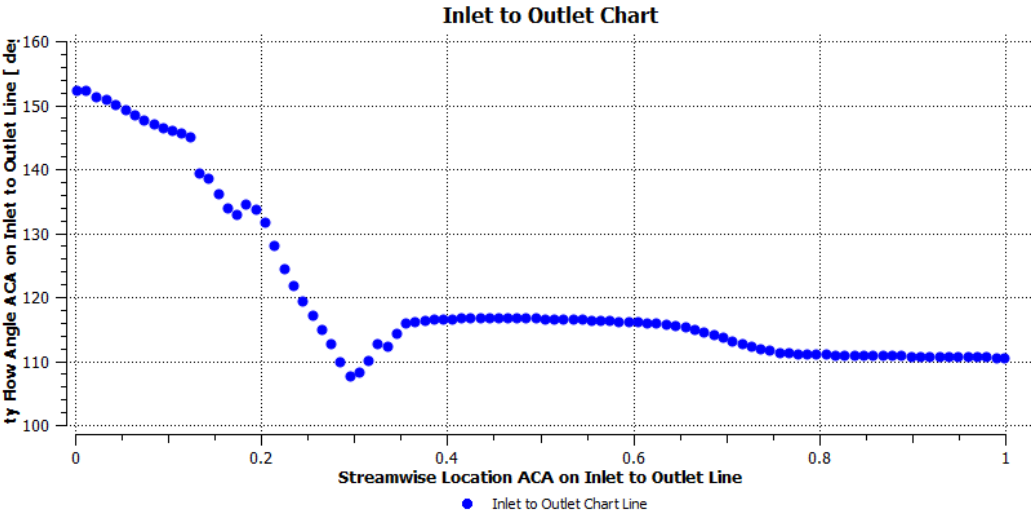

Figure 5.15 Streamwise Flow Angle Chart (EAML EF=2)

5.4.4. EAML of Ellipse Factor 0.5 with 30 for the Real Hub

As it became obvious that ellipse should be developed at the opposite direction, and 0.5 factor was first selected (it would be like the circular blade

would be ‘stretched’ in radial dicrection by a factor 2). The results show that the flow angle at the outlet of the domain is 8.33 degrees and the total pressure loss is 8.51%. The results are significantly improved, encouraging in following this path in the detailed blade design.

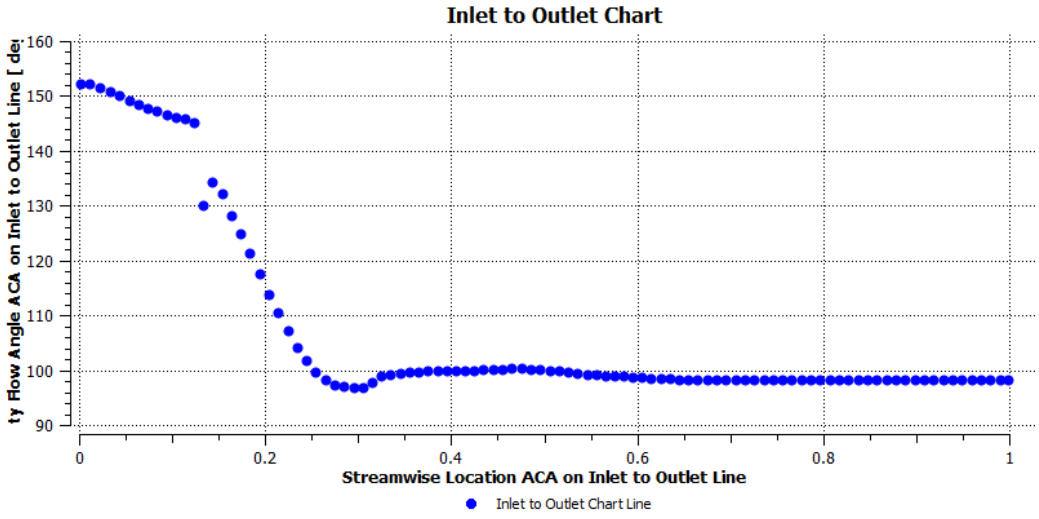

Figure 5.16 Streamwise Flow Angle (EAML EF=0.5)

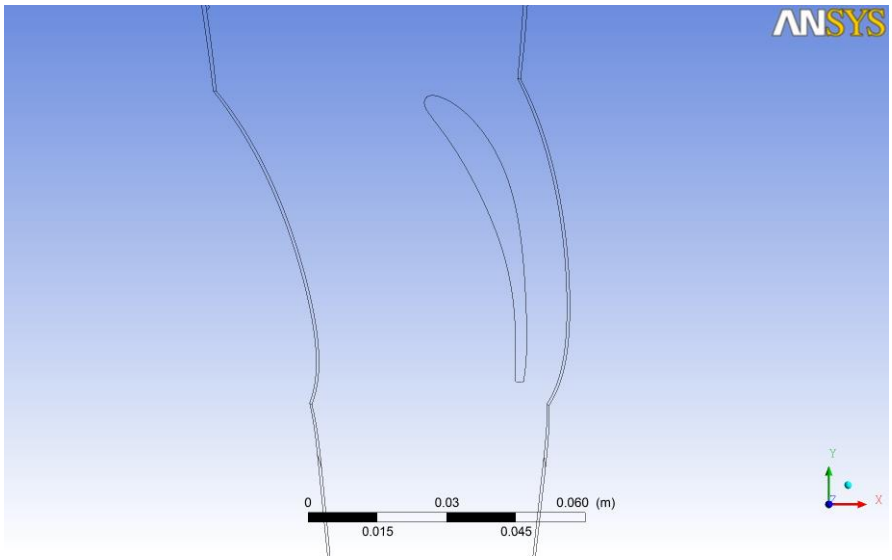

Figure 5.17 Profile View of the EAML Blade with an Ellipse Factor = 0.5 (30-Blade Configuration)

5.4.5. EAML of Ellipse Factor 0.65 with 30 and 60 Blades with Reduced Thickness

Although EAML blade with the ellipse factor of 0.5 performed well from the point of view of flow angle, an area with flow separation and irregularities was observed around the suction side of the blade. To overcome this problem, it was decided to approach the circle mean line again with a factor of 0.65 and to reduce the thickness of the blade for decreasing the pressure losses. The obtained results from the computation show that flow angle is 9.37 and 5.83, while the total pressure loss is 9.37% and 11.83 %, respectively, for the configurations with 30 and 60 blades. The chart of the streamwise low angle values are presented in Figure 5.18.

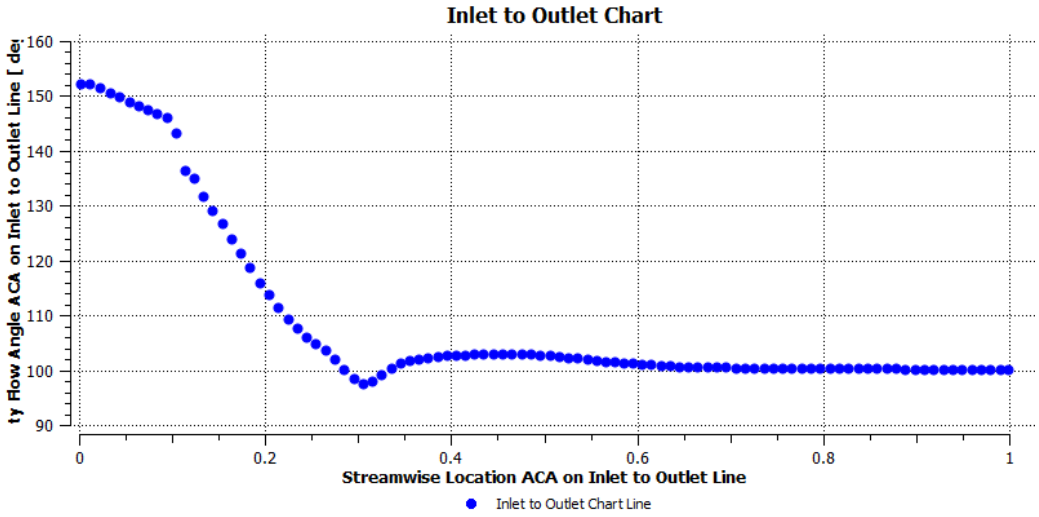

Figure 5.18 Streamwise Flow Angle (EAML EF=0.65)

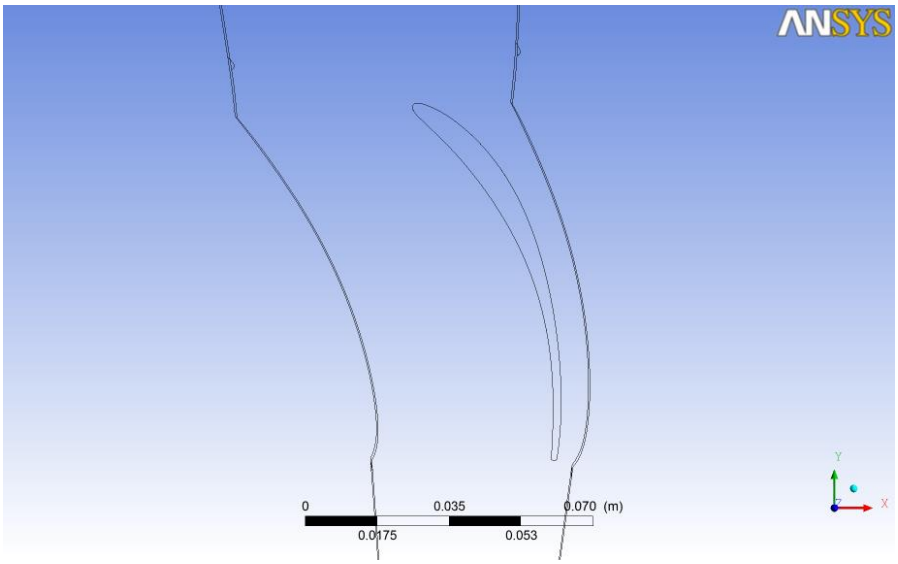

Figure 5.19 Profile View of the EAML Blade with an Ellipse Factor = 0.65 and reduced thickness (30-Blade Configuration)

5.4.6. EAML of Ellipse Factor 0.65 with 30 and 60 Twisted Blades

As stated the previous case the residual flow angle at the outlet of the flow channel couldn't be eliminated. Thus the idea of using twisted blades instead of blades with a constant profile throughout the spanwise direction was applied.

The results were 7.70 and 4.92 degrees for the flow angle and 7.3% and 8.49% for the total pressure loss, respectively, for 30 and 60 blade configurations.

Although the twisting of the blades affected the results in a positive way by decreasing the flow angle at the outlet, the effect was not significant and by considering the high cost of manufacturing the idea of the application of the twisted blades was abandoned.

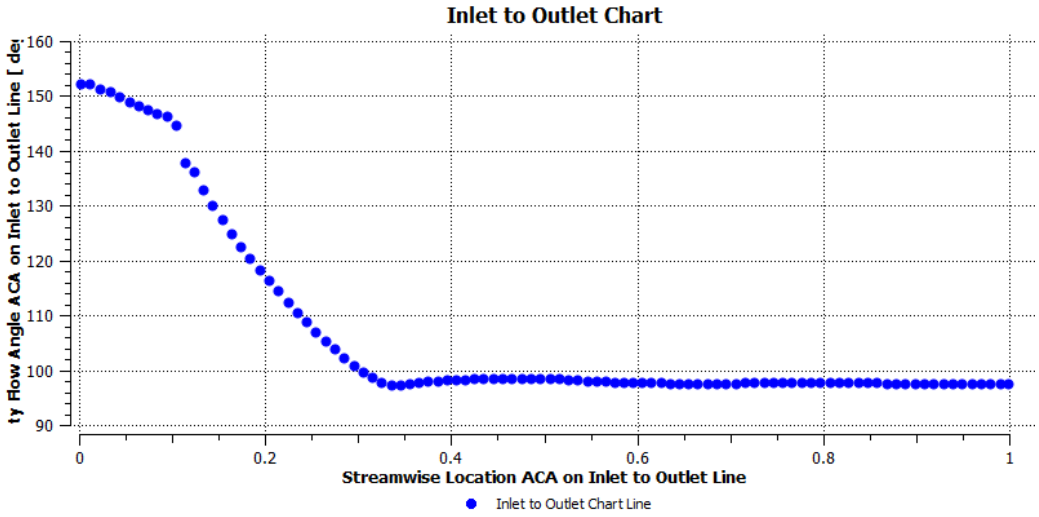

Figure 5.20 Streamwise Flow Angle (Twisted-EAML)

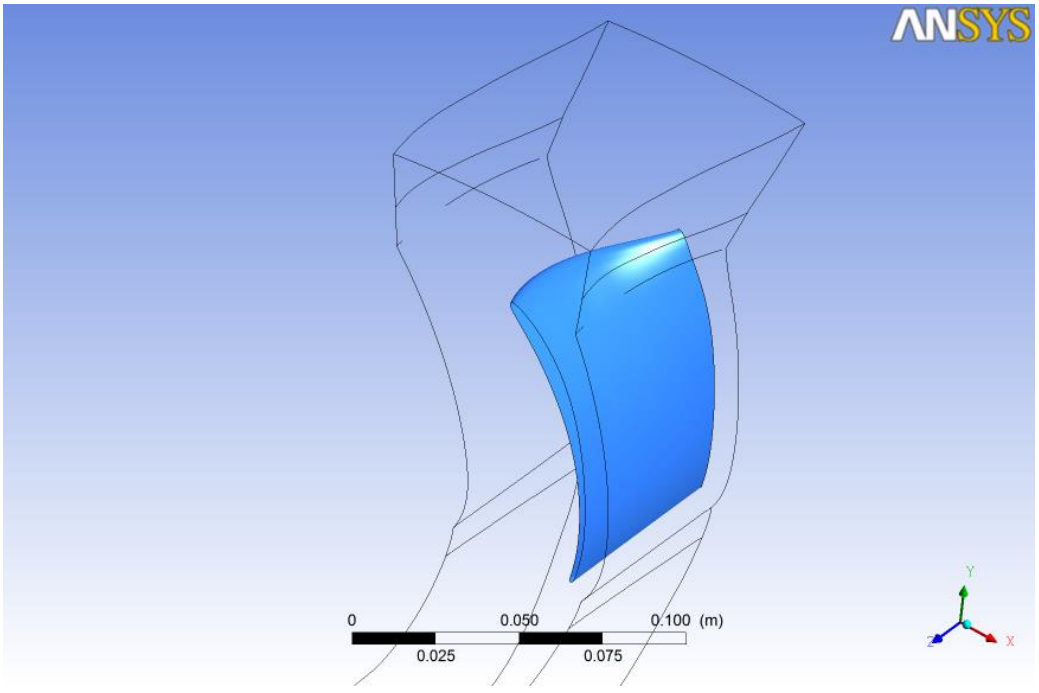

Figure 5.21 A View of the Twisted Blade

5.4.7. EAML of Ellipse Factor 0.65 with 30 Blades with Splitter Blades

As the twisted blades were found not worth for the final solution, another approach was tried by putting splitter blades besides the main blades. This allows achieving a configuration close to the one with 60 blades, allowing for a much more manufacture and installation. The radial chord of the splitter blades was defined considering the constraint of the distributor; the inlet geometric angle was determined on the basis on the prediction of the flow within the blade channel derived from previous simulations. The splitter blades were positioned in the middle of the pitch between the two blades, as after a few trials with different positions this was realized to be the optimum position to put the splitter blade in order to decrease the flow angle. It was observed that while the splitter blades ensured the same decrease in the outlet flow angle as in the case of 60 blades, the pressure loss was smaller. The results obtained from the simulation with the splitter blades are; 4.91 degrees for the flow angle and 10.23% for the total pressure loss. The Figures 5.22 and 5.23 show the streamwise flow angle chart of the simulation and the position of the splitter blade with respect to the main blade at midspan total pressure distribution.

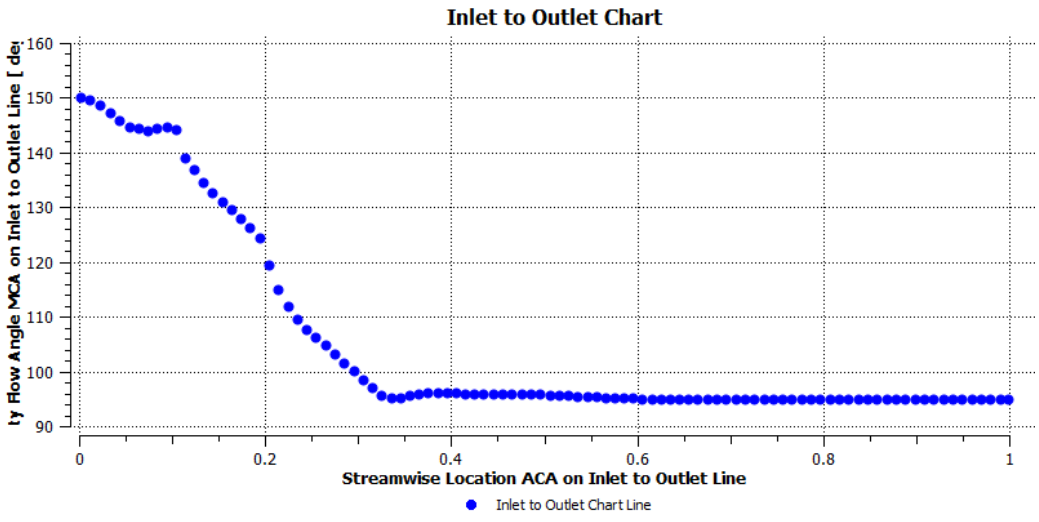

Figure 5.22 Streamwise Flow Angle (EAML with Splitter)

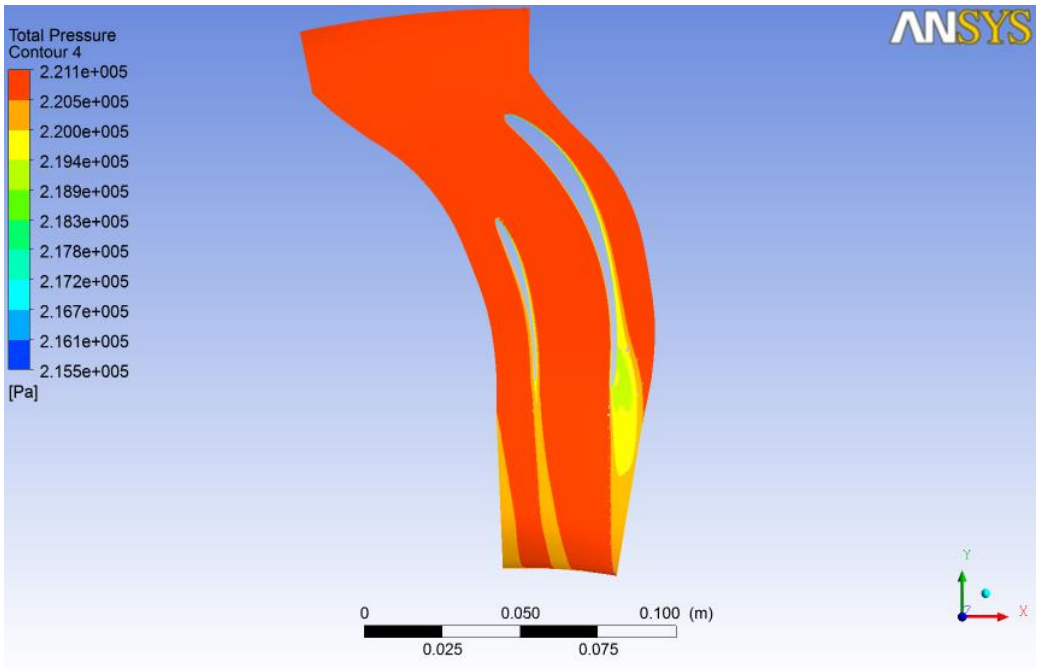

Figure 5.23 Total Pressure Distribution at midspan (EAML with Splitter)

5.4.8. EAML of Ellipse Factor 0.65 with 30 Blades with Splitter Blades, Modified Trailing Edge

Since even adding splitter blades to the configuration does not reduce the flow angle after a certain degree, the final decision to eliminate this residual angle was turning the trailing edge to have a geometric angle of negative values. After some trials it was found that -6 degrees turning at the trailing edge was able to give the desired result with -0.41 degrees at the outlet. The total pressure loss for this case was 8.91%. Also as the work was coming close to final stages, the y^+ value was adjusted to be 1 to increase the accuracy greatly especially in the boundary layer.

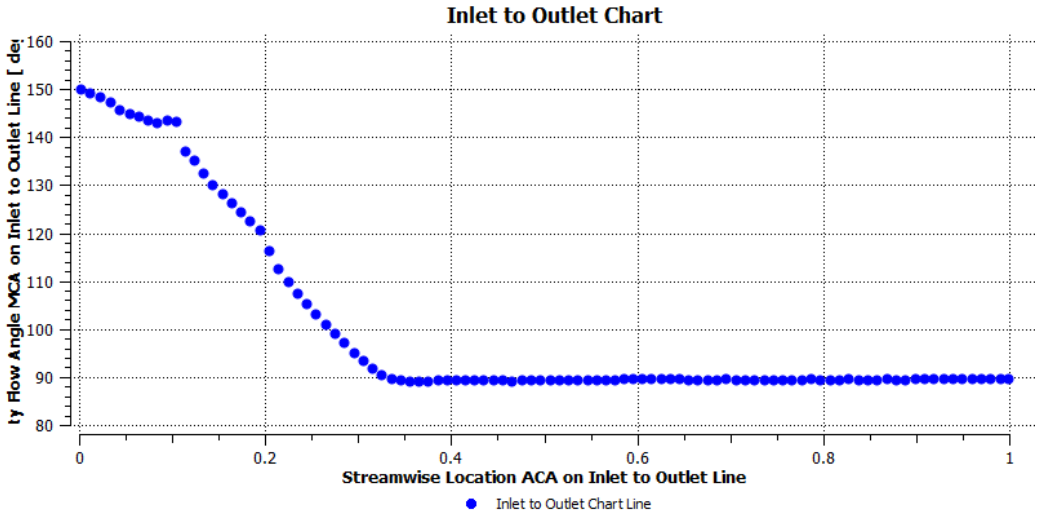

Figure 5.24 Streamwise Flow Angle (Modified EAML)

5.4.9. EAML of Ellipse Factor 0.65 with 30 Blades with Thickness Distribution of NACA0015, Modified Trailing Edge and increased accuracy (y^+ = 1)

After the mean line, blade length and trailing edge angle were defined, it was decided to increase the thickness of the blade for practical reasons such as the large variation of incidence angle in spanwise and pitchwise direction. Thickness distribution of NACA0015 was used on the already fixed mean line to create a thicker blade, with the thickness values based on [19]:

$$y_t = \frac{T}{0.2}\left(a_0 x^{0.5} + a_1 x + a_2 x^2 + a_3 x^3 + a_4 x^4\right) \qquad (5.1)$$

Where y_t is the half thickness at a given value of x which is the position along the chord as a fraction of the chord (0 to c) and T is the maximum thickness as a fraction of the chord (100xT gives the last two digits in the NACA 4-digit denomination.) . The constants are;

a_0 = 0.2969, a_1 = -0.126, a_2 = -0.3516, a_3 = 0.2843, a_4 = -0.1015 or for a closed trailing edge a_4 = -0.1036

The simulation was performed without splitter blades and it was found that the flow angle is 5.53 degrees and the total pressure loss is 8.54%. The

Figures 5.25 and 5.26 present the streamwise flow angle variation and the spanwise total pressure loss. The total number of elements in the computational domain was also increased (789400 hexahedral elements) compared to the previous simulations for a further increase in the accuracy. In the Figure 5.27 the streamlines from inlet to outlet can be observed.

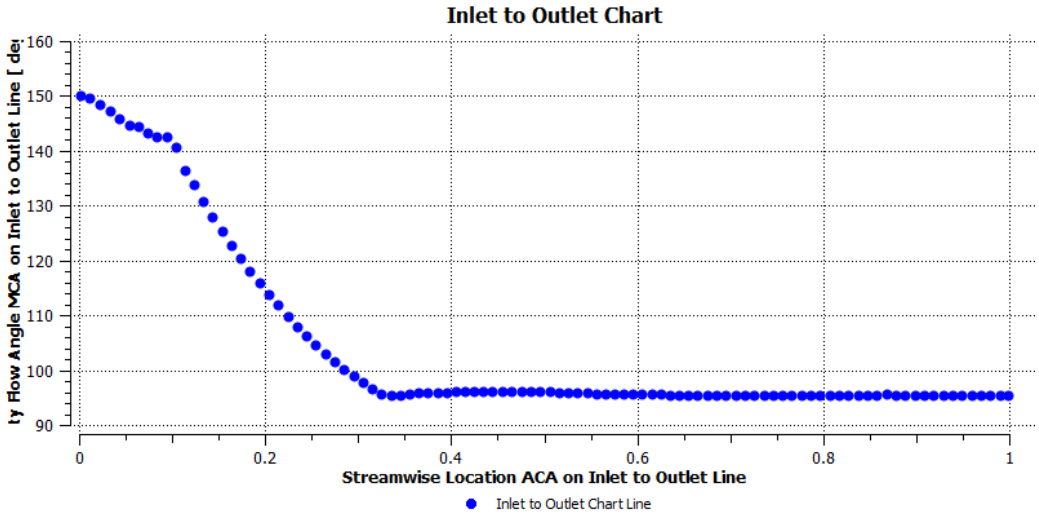

Figure 5.25 Streamwise Flow Angle (Final Design)

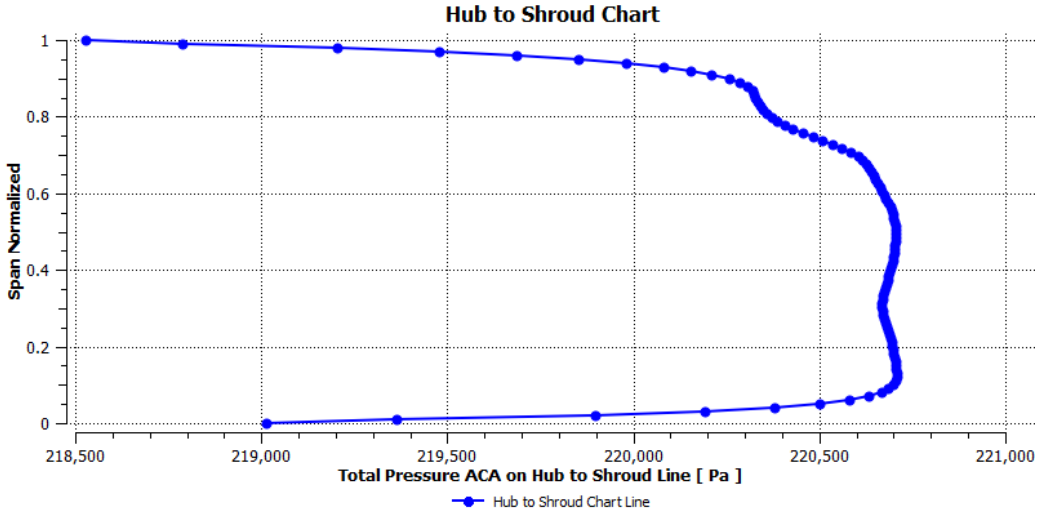

Figure 5.26 Spanwise Total Pressure Variation at Normalized Streamwise Position of 0.99 (Final Design)

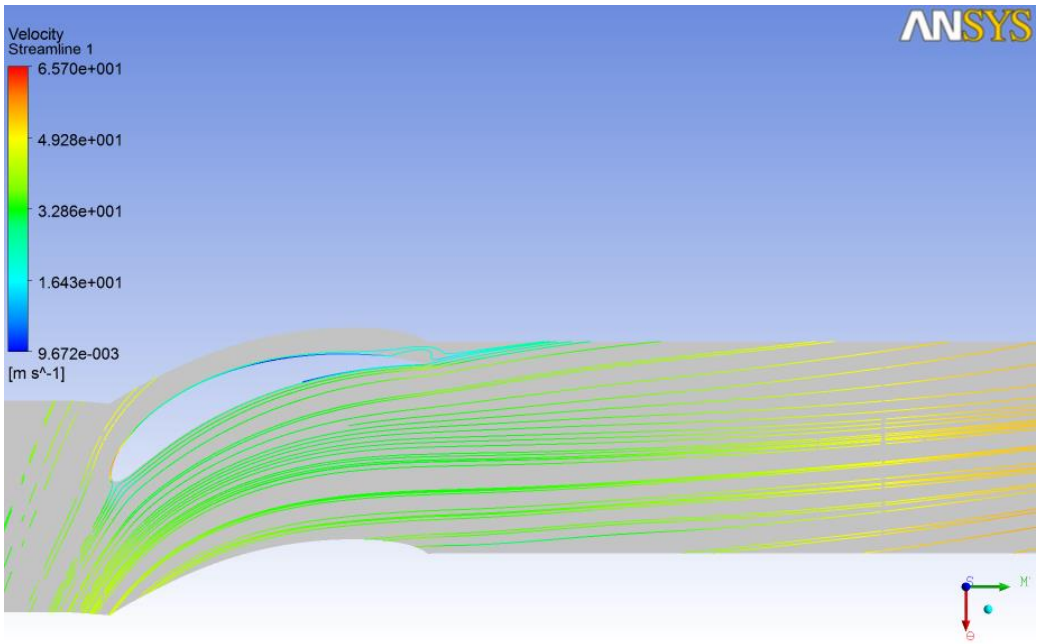

Figure 5.27 Streamlines at midspan (Final Design)

Considering the results of the final simulations that can be seen in Table 5.1, this case was chosen to be the final configuration on which the manufacturing will be based. Although with the splitter blades and the with the modification of the trailing edge it was possible to reduce the flow angle to values near zero, it was seen that in every case simulated there is a high flow angle variation in the spanwise direction that cannot be eliminated. This issue can be solved only by putting a honeycomb structure at the exit of the volute channel, upstream of the axial turbine. This solution would both eliminate the spanwise variation of flow angle and the mean residual flow angle which was 5.53 degrees at the expense of increasing the losses due to the elimination of the velocity components of the flow.

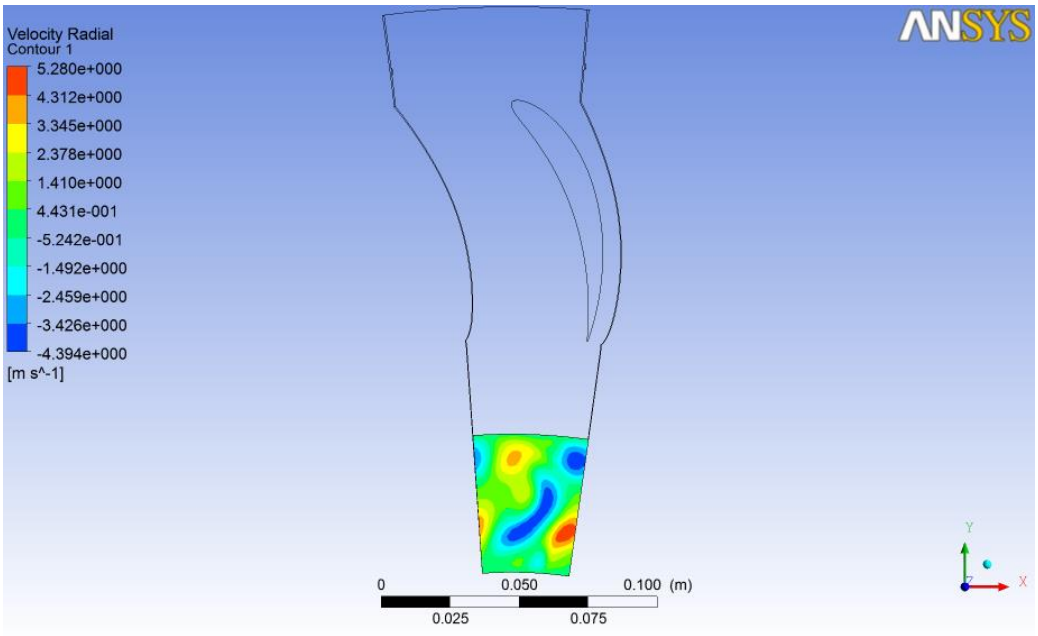

Figure 5.28 Radial Velocity Variation at Outlet (Final Design)

In Figure 5.28, variation in radial velocity which is an indicator of vortices at the outlet section is seen. Although the magnitude of the radial component of the velocity at the outlet is smaller than the circumferential component, it is also important to eliminate the radial component of the velocity in order to avoid vortices at the inlet of the axial turbine. Honeycomb structure will also solve this issue, and allows for a simpler IGV configuration with 30 blades manufactured according the optimal shape resulting at the end of this study.

5.5. Results

Case Name	Bladeset Number	Blade Radial Chord (mm)	R_inlet [mm]	R_outlet [mm]	Geometric Angle in (LE) (°)	Geometric Angle out (TE) (°)	Mean Yaw Angle (°)	Maximum/Minimum Yaw Angle (°)	Maximum Radial Angle (°)	Minimum Radial Angle (°)	Total Pressure Loss (%)
Original IGV (-15 °)	30	62	312	250	-15	-15	-20.9985	-14/-23.5	5.30	-5.90	33.408
Original IGV (+15 °)	30	62	312	250	15	15	20.82	18/4	10.33	-7.42	17.175
CAML	30	60	310	250	60	0	13.69	17.25/3.5	9.56	-7.08	7.951
CAML	60	60	310	250	60	0	9.6849	13/1	1.73	-1.38	17.636
EAML - medium cell number	30	60	310	250	60	0	17.63	24.5/5	5.11	-4.89	7.739
EAML - medium cell number	60	60	310	250	60	0	12.667	21/1	3.62	-4.27	16.343
EAML - modified outlet	30	60	310	250	60	0	14.976	19.5/4.5	7.22	-3.01	7.299
EAML - Ellipse Factor=4	30	60	310	250	60	0	20.73	23.5/10.5	3.28	-2.30	11.258
EAML - Ellipse Factor=2	30	60	310	250	60	0	18.143	21/8	5.08	-3.50	9.798
EAML - Ellipse Factor=0.5	30	60	310	250	60	0	8.4549	13.5/-1	9.54	-9.39	7.834
EAML - Ellipse Factor =0.5, Real Hub (all simulations are carried out for the real hub after this point)	30	60	310	250	60	0	8.3392	14/-1.5	9.67	-9.10	8.416
EAML - Ellipse Factor =0.5	60	60	310	250	60	0	4.5259	11.5/-4	2.48	-2.21	8.711

EAML - EF=0.65, thinner blade	30	73	320	247	60	0	10.28500	17/0.5	8.21	-7.63	10.320
EAML - EF=0.65, thinner blade	60	73	320	247	60	0	7.2648	11.5/-3	1.86	-2.01	14.956
EAML - EF=0.65, thinner blade @ TE	30	73	320	247	60	0	9.7397	15/0	8.07	-7.12	9.377
EAML - EF=0.65, thinner blade @TE	60	73	320	247	60	0	5.8335	11/-3	3.14	-3.57	11.838
EAML - EF =0.65, Twisted	30	85	320	235	60	0	7.7027	14/0	4.99	-6.23	7.312
EAML - EF =0.65, Twisted	60	85	320	235	60	0	4.9266	12.5/-1.75	2.14	-1.80	8.495
EAML - EF =0.65, Twisted	90	85	320	235	60	0	4.0238	10/-1	1.33	-1.39	10.938
EAML - EF=0.65, thinner+longer blade	30	85	320	235	60	0	8.7465	14.25/-1	9.69	-8.22	8.394
EAML - EF=0.65, thinner+longer blade (fixed after this point)	60	85	320	235	60	0	5.5094	10/-4	3.00	-3.40	13.288
EAML with splitter (pitchwise splitter position = -4.77 degrees)	30	85	320	235	60	0	5.0062	10/-1.5	5.81	-4.77	9.470
EAML with splitter (pitchwise splitter position = -6 degrees/halfway)	30	85	320	235	60	0	4.9149	11/-2.75	6.50	-5.35	10.234
EAML with splitter (pitchwise splitter position = -8 degrees)	30	85	320	235	60	0	6.7168	10.5/-2.25	9.37	-10.00	11.496

EAML with splitter (pitchwise splitter position = -6 degrees/halfway) with increased thickness	30	85	320	235	60	0	7.5753	12/-2	3.94	-4.12	11.377
EAML with splitter (pitchwise splitter position = -6 degrees/halfway), Trailing Edge: -5 °	30	85	320	235	60	-5	2.9181	8.5/-7	4.12	-4.58	12.696
EAML with splitter (pitchwise splitter position = -6 degrees/halfway), Trailing Edge: -10 °	30	85	320	235	60	-10	-2.53	3.5/-10	8.89	-4.78	8.313
EAML with splitter (pitchwise splitter position = -6 degrees/halfway), Trailing Edge: -10 ° , y+=1	30	85	320	235	60	-10	-3.38	2/-9.75	8.73	-5.72	8.855
EAML with splitter (pitchwise splitter position = -6 degrees/halfway), Trailing Edge: -7 ° , y+=1	30	85	320	235	60	-7	-1.1592	6/8.25	6.00	-4.59	8.829
EAML with splitter (pitchwise splitter position = -6 degrees/halfway), Trailing Edge: -6 ° , y+=1	30	85	320	235	60	-6	-0.4196	7/-7.5	5.08	-5.15	8.911
NACA 65S	30	85	320	235	60	0	12.598	18/1	5.61	-3.55	11.040
NACA 65S - TE:-16	30	85	320	235	60	-16	1.7031	8.5/-11	7.34	-6.41	11.354
NACA 65S - TE:-16	60	85	320	235	60	-16	-3.3684	2/-19	2.05	-2.41	20.873

EAML+A3K7 Thickness distribution - TE:-6 ° y+=1	30	85	320	235	60	-6	-3.6485	6/-13	6.61	-5.52	13.426
EAML+A3K7 Thickness distribution with splitters- TE:-6 ° y+=1	30	85	320	235	60	-6	-0.8679	7/-10	7.23	-5.58	15.693
EAML+NACA0015Thickness distribution - y+=1	30	85	320	235	60	0	9.7378	15.5/1.5	7.16	-8.94	8.560
EAML+NACA0015 Thickness distribution - TE:-6 ° y+=1	30	85	320	235	60	-6	5.5339	12.5/-3	5.67	-4.72	8.541
NACA0015 - TE:-5 ° y+=1	30	85	320	235	60	-5	6.7085	13/-3.5	7.14	-7.83	10.485

Table 5.1 Simulation Results

Chapter 6

Conclusion

This thesis has discussed a wide set of numerical investigations aimed at developing a base profile for the inlet guide vanes that will be used in an experimental campaign about axial flow turbine stages. The objective of the study was to achieve an as uniform as possible axial flow at the discharge of a centripetal distributor. The inlet guide vanes will be positioned radially in the distributor of the axial stage of the high speed closed loop test rig in the Laboratorio di Fluidodinamica delle Macchine in Politecnico di Milano.

The work is completed in two main steps:

1. Design and Modeling of the Distributor: The flow region inside the distributor of the axial test turbine was modeled at this stage to see the behavior of the flow inside without any IGV, and to determine the characteristics of the flow at the inlet section of the IGVs. It was seen that the yaw angle upstream of the IGV reaches a very high value, close to 70 degrees; the same flow angle is predicted at the exit of the distributor if IGVs are not installed. The second stage of the work was based on these information, that will be used as design indication for the geometry of the blade. It was also seen that the original IGVs designed to be used in the distributor were highly inefficient in directing the flow, resulting in yaw angle over 20 degrees, and were creating large total pressure losses leading to a search for a new IGV design.
2. CFD Analysis of Different IGV Profiles: The main aim of this second step, mostly based on the knowledge gained in the first part about the flow behavior, is to finalize a blade design to obtain a uniform flow, which is the main goal of this study, by analyzing a number of profile types and configurations (including different solidity, splitter blade configuration, three-dimensional blade design). As the manufacturing cost of the blades and the simplicity of installation are also accounted for, the design was tried to be kept as simple as possible. Configurations with twisted and fully three-dimensional blades, 60 blades or splitter blades actually gave good

results with regards to the flow angle; however, due to the increased cost and complexity of these configurations and the impossibility of preventing both the spanwise fluctuation in the yaw angle and the vortices at the inlet of the axial turbine in any kind of configuration, these solutions were excluded in favor of using a simpler blade set composed by 30 IGVs, implementing the most efficient blade design and introducingan honeycomb structure at the end of the distributor.

As the final design, an Elliptic Arc Mean Line Blade was adopted. The thickness of the blade was derived from the thickness distribution of NACA0015 and the blade was modified to minimize the swirl angle at the turbine inlet. The simulations show that the final blade design results in 5.53 degrees of mean yaw angle, 8.54% total pressure loss and about 15 degrees of yaw angle variation in the spanwise direction. Due to the practical reasons that are mentioned above a honeycomb structure was decided to be used to eliminate the residual flow angle and spanwise variation at the expense of a slight increase in total pressure loss.

Appendix

1. **Fortran Code**
2. **Technical Drawings**

```
program Mean


implicit none

integer :: i,j,k,n,m,ncol

real    :: r,x0,y0

real                                                                    ::
Ps_oav,Pt_omav,vrad_omav,vtan_omav,vaxi_omav,yaw_omav,pit_omav,G,Gi
ncr

real, dimension(:,:,:), allocatable :: datum

real, dimension(:,:), allocatable :: theta, vaxi, vrad, vtan

real, dimension(:), allocatable :: Ps_av, Pt_av, vaxi_av, vrad_av, vtan_av,
yaw_av, pit_av

real, dimension(:), allocatable :: Pt_mav, vaxi_mav, vrad_mav, vtan_mav,
yaw_mav, pit_mav

character(50) :: datafile

open(unit=1,file='input.inf')

read(1,'(a)')datafile

read(1,*)r

read(1,*)x0

read(1,*)y0

read(1,*)n

read(1,*)m

read(1,*)ncol

close(1)

allocate(datum(n,m,ncol),theta(n,m),vrad(n,m),vtan(n,m),vaxi(n,m))
```

```
allocate(Ps_av(m),Pt_av(m),vaxi_av(m),vrad_av(m),vtan_av(m),yaw_av(m),pit
_av(m))

allocate(Pt_mav(m),vaxi_mav(m),vrad_mav(m),vtan_mav(m),yaw_mav(m),pit
_mav(m))

open(unit=1,file=datafile)

read(1,*)

read(1,*)

read(1,*)

do j = 1, m

  do i = 1, n

    read(1,*)(datum(i,j,k),k=1,ncol)

    theta(i,j) =  atan2((datum(i,j,2)-y0),(datum(i,j,1)-x0))

!     print*,i,j,datum(i,j,2),datum(i,j,1),theta(i,j)

    vrad(i,j)  =  datum(i,j,6)*cos(theta(i,j)) + datum(i,j,7)*sin(theta(i,j))

    vtan(i,j)  =  datum(i,j,6)*sin(theta(i,j)) - datum(i,j,7)*cos(theta(i,j))

    vaxi(i,j)  =  datum(i,j,8)

  enddo

!   pause

enddo

close(1)

! aritmetic averages

Ps_av = 0.

Pt_av = 0.

vrad_av = 0.
```

```
vtan_av = 0.
vaxi_av = 0.
do j = 1, m
  do i = 1, n
    Ps_av(j)   =  Ps_av(j) + datum(i,j,4)
    Pt_av(j)   =  Pt_av(j) + datum(i,j,5)
    vrad_av(j) =  vrad_av(j) + vrad(i,j)
    vtan_av(j) =  vtan_av(j) + vtan(i,j)
    vaxi_av(j) =  vaxi_av(j) + vaxi(i,j)
  enddo
  Ps_av(j)   =  Ps_av(j)/n
  Pt_av(j)   =  Pt_av(j)/n
  vrad_av(j) =  vrad_av(j)/n
  vtan_av(j) =  vtan_av(j)/n
  vaxi_av(j) =  vaxi_av(j)/n
enddo
yaw_av(:) = atan2(vtan_av(:),abs(vrad_av(:)))*180/3.141593
pit_av(:) = atan2(vaxi_av(:),sqrt(vrad_av(:)**2+vtan_av(:)**2))*180/3.141593
open(unit=1,file='circ_av.dat')
write(1,'(a)')'variables= "Z [ m ]" "Pressure [ Pa ]" "Total Pressure [ Pa ]" "Vrad
[ m s^-1 ]" "Vtan [ m s^-1 ]" "Vaxi [ m s^-1 ]" "Yaw [deg]" "Pitch [deg]"'
do j = 1, m
write(1,113)datum(1,j,3),Ps_av(j),Pt_av(j),vrad_av(j),vtan_av(j),vaxi_av(j),yaw
_av(j),pit_av(j)
```

```
enddo
close(1)
! mass averages
Pt_mav = 0.
vrad_mav = 0.
vtan_mav = 0.
vaxi_mav = 0.
do j = 1, m
  do i = 1, n
    Pt_mav(j)   =  Pt_mav(j) + datum(i,j,5)*vrad(i,j)
    vrad_mav(j) =  vrad_mav(j) + vrad(i,j)*vrad(i,j)
    vtan_mav(j) =  vtan_mav(j) + vtan(i,j)*vrad(i,j)
    vaxi_mav(j) =  vaxi_mav(j) + vaxi(i,j)*vrad(i,j)
  enddo
  Pt_mav(j)   =  Pt_mav(j)/vrad_av(j)/360
  vrad_mav(j) =  vrad_mav(j)/vrad_av(j)/360
  vtan_mav(j) =  vtan_mav(j)/vrad_av(j)/360
  vaxi_mav(j) =  vaxi_mav(j)/vrad_av(j)/360
enddo
yaw_mav(:) = atan2(vtan_mav(:),abs(vrad_mav(:)))*180/3.141593
pit_mav(:)                                                    =
atan2(vaxi_mav(:),sqrt(vrad_mav(:)**2+vtan_mav(:)**2))*180/3.141593
open(unit=1,file='circ_mav.dat')
```

```
write(1,'(a)')'variables= "Z [ m ]" "Pressure [ Pa ]" "Total Pressure [ Pa ]" "Vrad
[ m s^-1 ]" "Vtan [ m s^-1 ]" "Vaxi [ m s^-1 ]" "Yaw [deg]" "Pitch [deg]"'

do j = 1, m

write(1,113)datum(1,j,3),Ps_av(j),Pt_mav(j),vrad_mav(j),vtan_mav(j),vaxi_ma
v(j),yaw_mav(j),pit_mav(j)

enddo

close(1)

! mean overall

Ps_oav = 0.

Pt_omav = 0.

vrad_omav = 0.

vtan_omav = 0.

vaxi_omav = 0.

G = 0.

do j = 1, m-1

  Ps_oav = Ps_oav + (Ps_av(j+1)+Ps_av(j))/2 * (datum(1,j+1,3)-
datum(1,j,3))

  Gincr = (vrad_av(j+1)+vrad_av(j))/2 * (datum(1,j+1,3)-datum(1,j,3))

  Pt_omav = Pt_omav + (Pt_mav(j+1)+Pt_mav(j))/2 * Gincr

  vrad_omav = vrad_omav + (vrad_mav(j+1)+vrad_mav(j))/2 * Gincr

  vtan_omav = vtan_omav + (vtan_mav(j+1)+vtan_mav(j))/2 * Gincr

  vaxi_omav = vaxi_omav + (vaxi_mav(j+1)+vaxi_mav(j))/2 * Gincr

  G = G + (vrad_av(j+1)+vrad_av(j))/2 * (datum(1,j+1,3)-datum(1,j,3))

enddo
```

```
Ps_oav    =  Ps_oav/(datum(1,m,3)-datum(1,1,3))

Pt_omav   =  Pt_omav/G

vrad_omav  =  vrad_omav/G

vtan_omav  =  vtan_omav/G

vaxi_omav  =  vaxi_omav/G

yaw_omav = atan2(vtan_omav,abs(vrad_omav))*180/3.141593

pit_omav                                                    =
atan2(vaxi_omav,sqrt(vrad_omav**2+vtan_omav**2))*180/3.141593

open(unit=1,file='circ_oav.dat')

write(1,'(a)')'variables= "Pressure [ Pa ]" "Total Pressure [ Pa ]" "Vrad [ m s^-1
]" "Vtan [ m s^-1 ]" "Vaxi [ m s^-1 ]" "Yaw [deg]" "Pitch [deg]"'

write(1,113)Ps_oav,Pt_omav,vrad_omav,vtan_omav,vaxi_omav,yaw_omav,pit
_omav

close(1)

print*,Ps_oav,Pt_omav,vrad_omav,vtan_omav,vaxi_omav,yaw_omav,pit_omav

pause

113 format(15f15.4)


end program
```

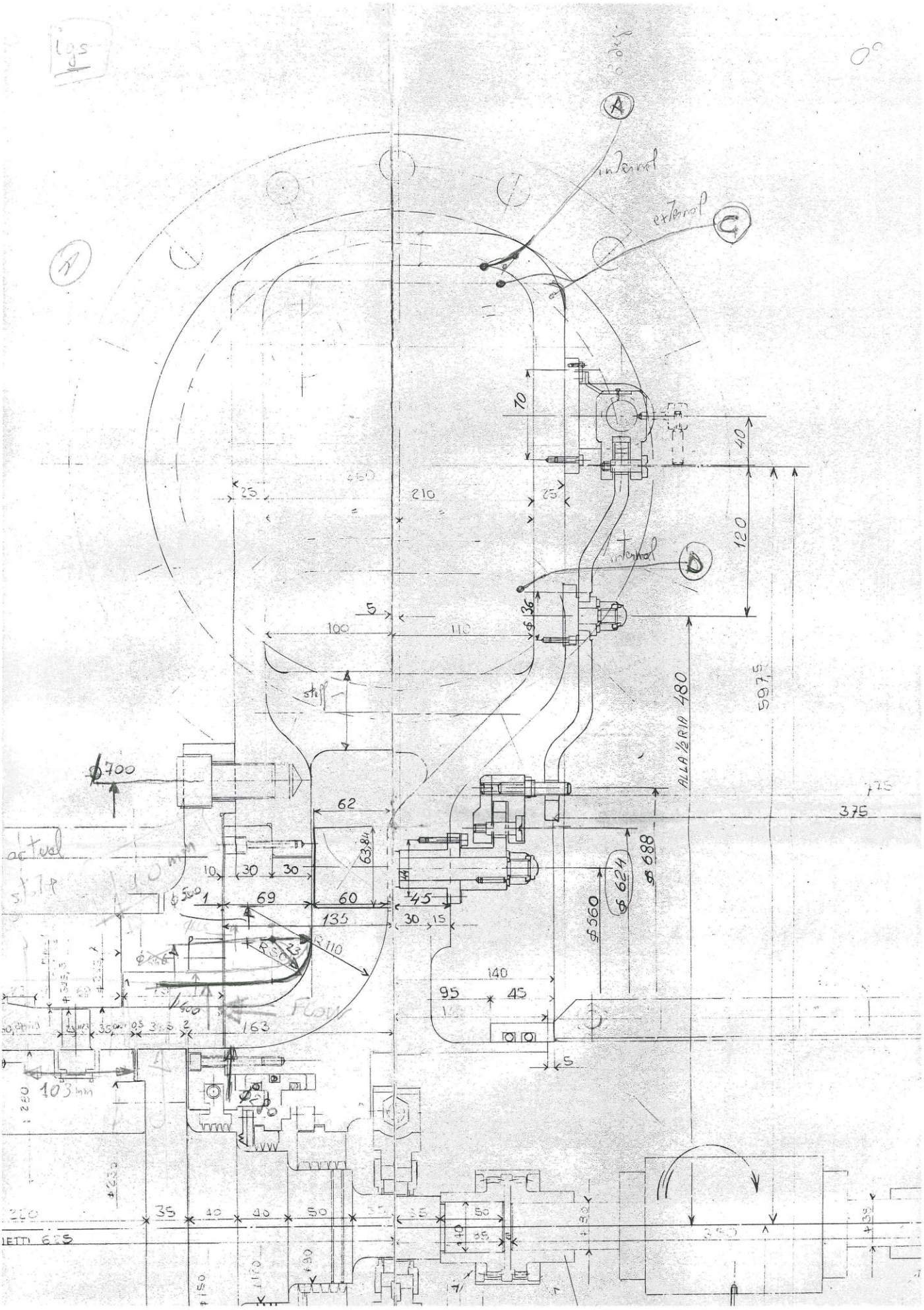
internal
external
internal
stiff
Flow
ALLA 1/2 RIB 480
597.5
375
210
100
110
140
95
45
163
103mm
Φ700
Φ560
Φ624
Φ688
R50
R110

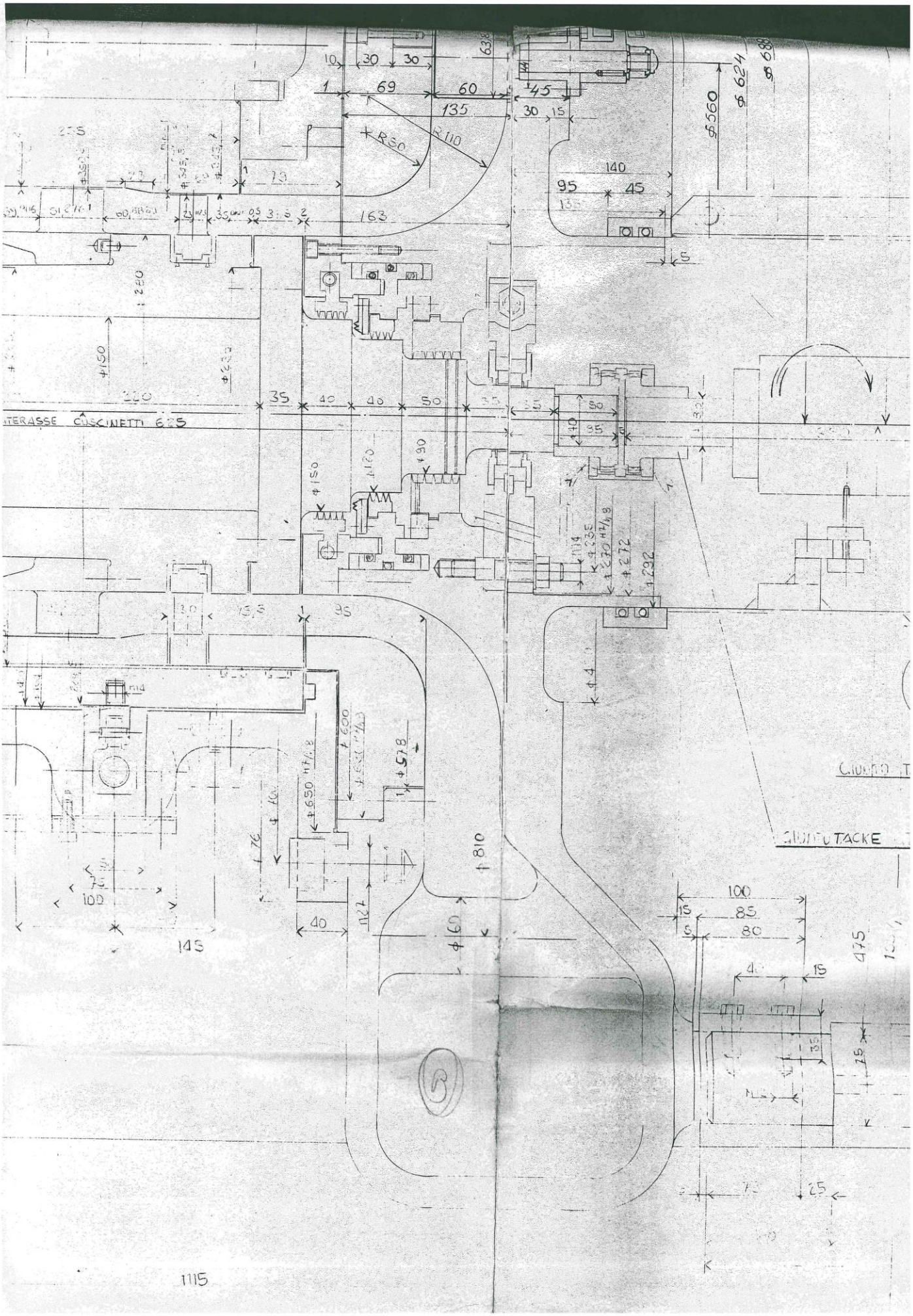
TERASSE CUSCINETTI 625
1115

Bibliography

[1] C. B. Meher-Homji, *The Historical Evolution of Turbomachinery,* Proceedings of the 29th Turbomachinery Symposium, pp. 281-322, 2000

[2] A. Lazzaretto, A. Toffolo, *Analytical and Neural Network Models for Gas Turbine Design and Off-Design Simulation,* International.Journal of Applied Thermodynamics, Vol.4, (No.4), pp.173-182, December-2001

[3] Jichao Li, Feng Lin, Chaoqun Nie, Jingyi Chen, *Automatic Efficiency Optimization of an Axial Compressor with Adjustable Inlet Guide Vanes*, Journal of Thermal Science Vol.21, No.2, 120-126, 2012

[4] Schott et al., *Inlet Guide Vane,* United States Patent, No US 7,985,053 B2, July 26 2011

[5] H. K. Versteeg, W. Malalasekera, *An Introduciton to Computational Fluid Dynamics,*Longman Scientific and Technical, 1995

[6] C. Osnaghi: Teoria delle turbomacchine, Progetto Leonardo, Bologna (Ristampa Gennaio 2006)

[7] D. Dotti, *Numerical investigation on a super-aggressive inter-turbine diffuser*, Master Thesis, 2011

[8] S. L. Dixon: Fluid Mechanics and Thermodynamics of Turbomachinery, Elsevier Butterworth Heinemann, Fifth edition, 1998

[9] G. B. Persico, *Tecniche di Modellazione delle Macchine a Fluido*, Lecture Notes

[10] P. K. Kundu, I. M. Cohen, D. R. Dowling, *Fluid Mechanics*, Academic Press, Fifth Edition, 2011

[11] T. Von Karman, *Mechanical Similitude and Turbulence*, Technical Memorandım No. 611, NACA, 1931

[12] Hyen-Jun Choi et al, *CFD validation of performance improvement of a 500 kW Francis turbine*, Renewable Energy 54, pp.111-123, 2013

[13] P.G. Tucker, *Trends in turbomachinery turbulence treatments*, Progress in Aerospace Sciences, 63, pp. 1-32, 2013

[14] ANSYS-CFX Guide

[15] http://www.lfm.polimi.it/facilities

[16] P. Gaetani, G. Persico, V. Dossena, C. Osnaghi, *Investigation of the Flow Field in a High-Pressure Turbine Stage for Two Stator-Rotor Axial Gaps—Part I: Three-Dimensional Time-Averaged Flow Field* ,Journal of Turbomachinery, Vol. 129 , pp.572-579 , July 2007

[17] F. R. Menter, *Zonal Two Equation k-ω Turbulence Models for Aerodynamic Flows*, AIAA Paper 93-2906, 1993.

[18] F. R. Menter, *Two-Equation Eddy-Viscosity Turbulence Models for Engineering Applications*, AIAA Journal, Vol. 32, No 8. pp. 1598-1605, 1994

[19] C. L. Ladson, C. W. Brooks, Jr., A. S. Hill, D. W. Sproles, *Computer Program To Obtain Ordinates for NACA Airfoils*, NASA Technical Memorandum 4741, December 1996